Focal Spot Optimization Using Spatial Light Modulation and a Phase Retrieval Algorithm

LUND
UNIVERSITY

Master's Thesis

by Robert Petersen

2023

Supervisor: Per Eng-Johnsson
Assistant supervisor: Cord Arnold
Examiner: Lars Rippe
LRAP: 592

Abstract

Aberrations to the wavefront of a laser beam reduce the quality of the focal spot and are generally undesired. This project is aimed at determining the aberrations of laser beams by using a phase retrieval algorithm and to show that it is possible to correct the aberrations with a spatial light modulator to optimize the focal spot. In particular, a two-dimensional phase pattern is retrieved and decomposed into Zernike polynomials to generate two distinct correction patters that are applied to the spatial light modulator to increase the peak intensity and reduce the width of the focal spot. Measurements of the aberrations of a terawatt laser are performed with the phase retrieval algorithm and compared to measurements with a Shack–Hartmann wavefront sensor.

Acknowledgements

Popular Science Summary

Removing the Aberrations from an Invisible Laser Beam

A laser beam can be focused to a spot to achieve an even higher intensity of the light, but aberrations of the beam increase the size of the focal spot and reduce the intensity and this project shows that the aberrations can be corrected.

A convex lens such as for example a magnifying glass can be used to focus light to a small spot which is called the focal spot. On a sunny day a magnifying glass can be used to burn a piece of paper by focusing the sunlight onto this paper. A larger magnifying glass can collect more light and leads to a higher intensity of the focused sunlight. It is not possible to focus all the light into one infinitely small spot. That would result in an infinitely high intensity in this point and that is not possible due to the laws of physics. The size of the focal spot also depends on the focal length of the lens and a magnifying glass with a shorter focal length can create a smaller focal spot with a higher intensity that burns the paper better.

It is possible to calculate the size of this focal spot by using formulas, but in reality the size of the focal spot is usually larger due to aberrations of the light that gets focused. The light that comes from the sun also does not reach the magnifying glass without aberrations and the same is true during night when we look at the stars. The stars twinkle and at every moment look a little bit different due to aberrations of the light that originate from the turbulent atmosphere of the earth. Astronauts flying outside the atmosphere do not see this twinkling and could also focus the starlight better with a lens or a curved mirror. This is one of the reasons why space telescopes are launched to outer space to capture images of the universe. It is exceptionally expensive to built space telescopes and to launch them to outer space and the maximum size of space telescopes is limited by the used rocket. A technology that is used in the largest ground-based telescopes is called adaptive optics. The aberrations that originate in our atmosphere are constantly measured and corrected by deforming a mirror to counteract the effects of the atmosphere. The telescope can then see the stars without any twinkling.

A deformable mirrors is also used in the laboratory at the Lund High-Power Laser Facility where the experimental work for this project was done. Even if the light from the infrared lasers propagate in vacuum and do do not twinkle, aberrations are still present in a laser beam. They can originate from the laser itself or be introduced by mirrors or lenses or other components in the setup that are not aligned perfectly. The aberrations do not change so quickly and if the aberrations are measured, they can be corrected with the deformable mirror. The laser beam then gets focused and the focal spot gets better if the aberrations from the beam are first removed. This

focused light is used to generate high-order harmonics that create invisible pulses in the extreme ultraviolet spectrum with a duration of just a few hundred attoseconds. 100 attoseconds is an incredibly short time that is 10 quadrillion times shorter than a single second. Even light that is so fast that it could theoretically orbit the earth more than 7 times during a single second merely travels a distance that is shorter than 0.0005 times the thickness of a human hair during 100 attoseconds.

In this project, the aberrations of the infrared terawatt laser are measured with two different methods and a separate setup is built to optimize the focal spot by correcting the aberrations with a spatial light modulator which is a device that is similar to a deformable mirror with many small pixels. One method to measure the aberrations of a laser beam is to use an expensive device which is called a Shack-Hartmann wavefront sensor. It is also possible to instead focus the laser beam with a lens or a curved mirror and to capture images before and behind the focal spot and to use an algorithm on a computer to calculate the aberrations of the beam. This is a much cheaper and accessible way to determine the aberrations of a laser beam because the beam just has to get focused and just one camera is needed. This project shows that it is possible to measure the aberrations of an infrared laser beam with a camera and the phase retrieval algorithm and that the measured aberrations in the beam can be corrected with a spatial light modulator to create an improved and smaller focal spot.

Table of Contents

Chapter 1

Introduction

1.1 Background and Motivation

An unaberrated Gaussian beam with a flat wavefront can with a parabolic mirror be focused to the smallest spot size that is physically possible and the focal spot has a Gaussian intensity profile. Aberrations of a beam lead to a deformation of the wavefront that results in a larger and non-Gaussian focal spot with a lower peak intensity. Aberrations in a laser beam can originate from misaligned optical components in a setup and examples for typical aberrations are astigmatism and coma.

For high-order harmonic generation in the 10 Hz laboratory of the Lund High-Power Laser Facility, laser pulses are focused into a gas to generate high-order harmonics. Aberrations of the infrared beam lead to aberrations of the generated high-order harmonics and the lower intensity of the driving field due to the aberrations leads to a lower yield of the high-order harmonics. Those aberrations are undesired and result in a lower intensity of the focused extreme ultraviolet light (XUV). A reduction of those aberrations is currently attempted with a deformable mirror and a measurement of the wavefront with a Shack-Hartmann wavefront sensor, but the improvements to the beam profile are thought to be limited.

The motivation for this project originates from the idea to measure the aberrations in a different way by using a phase retrieval algorithm and to compare the results from the phase retrieval algorithm with the measurements of the Shack-Hartmann wavefront sensor.

The main goal of this project is to show that a phase retrieval algorithm in conjunction with a camera can be used to measure the two-dimensional phase pattern of an infrared laser beam and that adaptive optics can be used to correct the aberrations and optimize the focal spot. In particular, a setup with an infrared diode laser is built and a spatial light modulator (SLM) is used to correct the aberrations.

1.2 Thesis Outline

Chapter 2 covers the theoretical background and emphasizes the theoretical concepts and components that are relevant to this project. Chapter 3 provides a description of the simulations, programming of the SLM and the experimental methods that are used to obtain the phase of the beams and explains how the aberrations are corrected with the SLM. The results of the simulations and initial tests of the SLM, measurements of the phase and the improvements to the focal spot are shown and discussed in Chapter 4. Chapter 5 concludes the project by summarizing the achieved results and providing an outlook on prospective next steps.

Chapter 2

Theory

2.1 Laser Physics

Laser stands for "light amplification by stimulated emission of radiation" and is based on the process of stimulated emission that dates back to Albert Einstein[1]. The first operation of a laser took until 1960 and was achieved by Theodore Maiman[2] and is based on the work of Arthur Schawlow and Charles Townes[3]. Today, lasers are not just indispensable in fields such as optical communication, manufacturing, medicine and fundamental research but also provide the basis for this project.

2.1.1 Stimulated Emission

A laser is usually constructed with a gain medium inside an optical cavity. The gain medium is pumped to generate exited states and the optical cavity can be built by using a highly reflective spherical mirror on each side of the cavity. The lowest energy level of an atom is called the ground state and occurs when all electrons occupy the lowest energy state E_0. If an electron absorbs a photon with the frequency ν and energy[4]

$$E_{ph} = h \cdot \nu \tag{2.1}$$

where h is Planck's constant, the electron can get excited if there is a state available and occupy the new energy state with the energy

$$E_1 = E_0 + E_{ph}. \tag{2.2}$$

The deexcitation of an electron back to the ground state leads to the emission of a photon with a frequency that corresponds to the energy difference between the states.

The emission can be spontaneous but also be induced by the interaction of a photon with the same energy as the emitted photon. That process is called stimulated emission and is the basis for lasers. The emitted photon will not just have the same energy as the photon that stimulated the emission, but it will also have the same phase, direction and polarization.[5] The radiation from a continuous laser is thus monochromatic and coherent.

A laser that is optically pumped with incoherent light must have at least three energy states because the probability for stimulated emission is equal to the probability for stimulated absorption and a population inversion could otherwise not be achieved.[6] If more electrons are in the exited state than the ground state, then an avalanche effect can be started and the radiation gets amplified for every pass through the gain medium. A small fraction of the light does not get reflected by the mirrors of the lasers and the light that passes through the mirror with the lower reflectivity forms a beam.

2.1.2 Gaussian Beam

The Gaussian beam is a solution of the paraxial Helmholtz equation[7]

$$\frac{\partial^2 A}{\partial x^2} + \frac{\partial^2 A}{\partial y^2} - i \cdot 2k \cdot \frac{\partial A}{\partial z} = 0 \tag{2.3}$$

with the complex envelope $A(\vec{r})$, the imaginary number i and the wavenumber k. The intensity distribution of the light that is emitted from a laser can often be described as a Gaussian beam and is given by[8]

$$I(\rho, z) = I_0 \cdot \left[\frac{w_0}{W(z)} \right]^2 \cdot e^{-\frac{2\rho^2}{W^2(z)}} \tag{2.4}$$

with the peak intensity I_0, the beam waist radius w_0, the axial position z, the beam radius $W(z)$ and the radial position ρ. The intensity is thus the highest in the center of the beam and decreases as a Gaussian function with an increasing radial distance ρ. The beam radius is never smaller than the beam waist radius and small beam waist radii lead to larger divergence angles. The half-angle of the divergence also depends on the wavelength λ and is given by[9]

$$\theta_0 = \frac{\lambda}{\pi \cdot w_0}. \tag{2.5}$$

The radius of curvature of a Gaussian beam is described by[10]

$$R(z) = z \cdot \left[1 + \left(\frac{z_R}{z} \right)^2 \right] \tag{2.6}$$

where z represents the distance from the beam waist and z_R is the Rayleigh range that is defined as[10]

$$z_R = \frac{\pi w_0^2}{\lambda}. \tag{2.7}$$

At the beam waist, the radius of curvature is undefined and the wavefronts are planar. The radius of curvature has a minimum value at a distance of one Rayleigh range from the beam waist and therefore the wavefronts are most strongly curved at this distance.

2.1.3 Ultrafast Optics

The Intense XUV Attosecond Physics beamline for high-order harmonic generation uses a terawatt laser. This high power can not be achieved continuously but just for very short times. Short pulses with a high intensity are generated by a combination of techniques.

The minimum value of the time-bandwidth product for a Gaussian pulse shape is[11]

$$\Delta t \cdot \Delta \nu = 0.441 \tag{2.8}$$

with the temporal width Δt and the spectral width $\Delta \nu$. A broad spectral bandwidth is thus needed for the generation of very short pulses. A pulse with a duration of 35 fs for example needs a spectral bandwidth of at least 12.6 THz.

Mode locking is a technique that can generate ultrashort pulses of light by locking the phase of multiple modes in a laser cavity.[12] The frequencies ν of the possible modes q in the cavity with the length L are spaced equidistantly and are determined by

$$\nu = q \cdot \frac{c}{2L}. \tag{2.9}$$

The number of possible modes depends on the bandwidth of the laser which is limited by the gain profile of the gain medium. Before mode locking is achieved, the modes oscillate with a random phase relation to each other. If a constant phase difference between the individual modes is achieved, periodical constructive interference of the modes leads to pulses with a repetition rate that corresponds to the round trip time in the cavity of the laser.

The high intensity of the ultrashort pulses leads to self-focusing in the gain medium of the laser which damages it.[13] A technique that avoids such damage by stretching the

pulse in time before the amplification was invented by Donna Strickland and Gérard Mourou and is called chirped pulse amplification.[14] Gratings or chirped mirrors are used to chirp or stretch an initially short pulse in time before the amplification which reduces the intensity and prevents damage of the gain medium. The amplification of the chirped pulse then increases the pulse energy. The subsequent compression of the chirped pulse leads to ultrashort pulses with a very high peak power.

2.1.4 Aberrations

For a monochromatic beam, an optical wavefront is the surface where the phase has the same value. An ideal wavefront for unfocused beams is often a planar wavefront. The phase is then constant across the entire beam profile and the light can be focused to the smallest possible spot as illustrated in Figure 2.1. A spherical lens introduces spherical aberration for light outside the paraxial region and plane wavefronts do not get focused to the smallest physically possible spot size that can be achieved with parabolic mirrors or aspheric lenses that are more difficult to manufacture.[15]
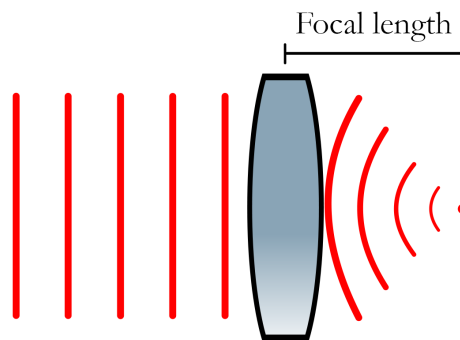
Figure 2.1: Schematic illustration of the focusing of an unaberrated wavefront by a lens

A parabolic curvature of the wavefronts would result in a focal spot that is shifted to a different position along the direction of the beam propagation. Tilted wavefronts would shift the focal spot to a different position in the focal plane. Aberrations of the beam lead to non-planar wavefronts and the size of the focal spot increases due to different tilts and curvatures of the wavefront at different positions across the beam profile.

2.2   Adaptive Optics

To correct aberrations of a laser beam, the aberrated wavefront has to be shaped so that the corrected wavefront is flat or has the desired curvature. Since a wavefront represents the surface with the same phase, a phase delay has to be added to the beam that cancels the aberrations at every point across the beam profile. This can be done by increasing the optical path length of the beam according to the aberrations across the beam profile.

2.2.1   Deformable Mirror

One way to increase the optical path length of a beam selectively across the beam profile is to reflect the beam from a deformed mirror that has a curvature of its surface that corrects the wavefront of the aberrated beam. A schematic two-dimensional representation of this principle is illustrated in Figure 2.2. The deformable mirror is curved according to the curvature of the aberrated wavefront and the angle of incidence of the beam. The reflected beam then has a flat wavefront without any aberrations. The mirror can additionally also be deformed to converge or diverge the beam and thus change the focal length of a setup by adding a radial symmetrical curvature to the reflected wavefront.
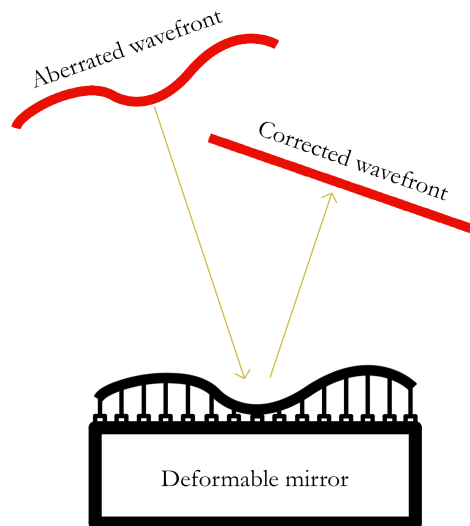

Figure 2.2: Schematic two-dimensional illustration of the correction of an aberrated wavefront by a deformable mirror

The deformation of the mirror is usually achieved by mechanically moving the reflective surface with individually controlled actuators. Although segmented deformable mirrors that are based on microelectromechanical systems[16] and liquid based deformable mirrors[17] exist, most deformable mirror technologies use a solid and continuous reflective surface that is deformed by the actuators positioned below. The reflective surface usually consists of at least one thin membrane that can be controlled by applying a magnetic or electric field to the individual actuators.

The deformable mirror that is used in this project is a bimorph deformable mirror with two layers of a piezoceramic material below a high reflection coated glass layer. The application of a voltage up to 350 V to electrodes expands the piezoceramic material due to the inverse piezoelectric effect and thereby also deforms the reflective surface. One layer out of the piezoceramic material is controlled by one electrode and used for the main curvature of the wavefront to shift the focus of the beam to the desired position behind the mirror. The other piezoceramic layer is controlled by 31 electrodes and used to correct the aberrations of the wavefront.

2.2.2 Spatial Light Modulation

SLMs are devices that modulate the phase, the intensity, the amplitude or the polarization of light across a one-dimensional or two-dimensional region and can be addressed electrically or optically.[18] They can either be transmissive or reflective and usually consist out of many individual pixels that can impart an independent modulation to the light. Many different technologies for spatial light modulation exist. SLMs can be based on the acousto-optic effect[19], the electro-optic effect[20], the magneto-optic effect[21], micromechanical arrays where every pixel can be moved individually[22] or the tilt of the molecules in liquid crystals[23]. Since a liquid crystal SLM that only modulates the phase is used in this project, this technology is explained in this section.

To correct aberrations by increasing the optical path length of the beam, it is not just possible to increase the geometrical path length as in the case of deformable mirrors. Liquid crystal SLMs modify the optical path length by changing the refractive index along the path of the light by rotating the molecules of liquid crystals. The molecules have an elongated shape and are as in usual liquids not ordered positionally but are ordered orientationally as in usual crystals.[24] The molecular orientation of the anisotropic molecules can be changed by an electric field due to torque that originates from induced dipoles and the electric forces.[25] An individual voltage across the liquid crystal layer can be applied to every pixel of the SLM which leads to a different rotation of the molecules in every pixel of the SLM.
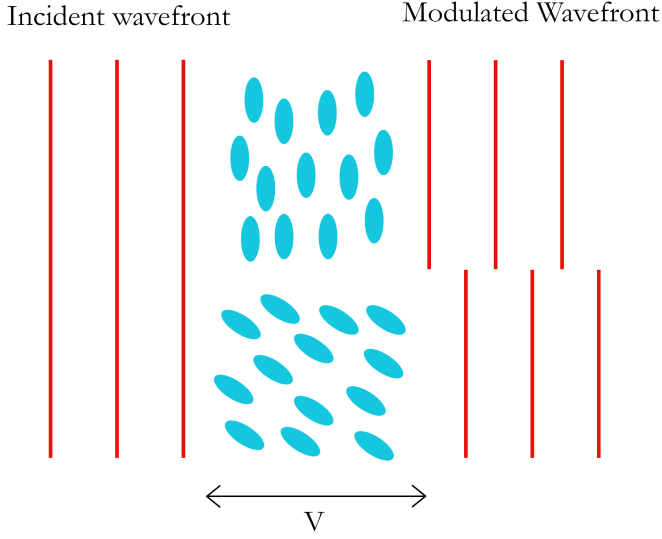
Figure 2.3: Schematic illustration of the phase modulation of liquid crystals depending on the applied voltage that changes the orientation of the liquid crystals

A birefringent uniaxial crystal has an ordinary refractive index n_o that is independent from the rotation angle θ and another refractive index that depends on the orientation of the crystal. That refractive index $n(\theta)$ can vary between n_o and the principal refractive index of one axis of the index ellipsoid n_e and is calculated by[26]

$$\frac{1}{n^2(\theta)} = \frac{\cos^2(\theta)}{n_e^2} + \frac{\sin^2(\theta)}{n_o^2}.$$ (2.10)

Linearly polarized light that is polarized parallel to the orientation of the untilted liquid crystal molecules is used for all later experiments and the phase shift of the modulated light then depends on the rotation angle θ and is described by[26]

$$\varphi = \frac{2\pi \cdot n(\theta) \cdot d}{\lambda_0}$$ (2.11)

with the distance of propagation in the liquid crystal layer d and the vacuum wavelength λ_0. Depending on the values of n_o and n_e, a different orientation of the liquid crystal molecules leads to a different phase shift and allows to modulate the phase independently for every pixel of the SLM by applying different voltages to the electrodes of every pixel.

A liquid crystal on silicon SLM (LCOS SLM) that is reflective is used in this project. It consists out of a silicon substrate, a dielectric mirror, a liquid crystal layer, alignment

films, transparent electrodes and a glass substrate.[27] The reflected modulated light traverses the liquid crystal layer twice. Part of the light is reflected from the glass substrate or other layers on top the liquid crystal layer without being modulated by the liquid crystals of the SLM. That light is called the zero-order reflection and it can be discriminated from the modulated light by applying an additional linear or spherical phase to the SLM.[28]

2.3   Zernike Polynomials

To describe wavefront aberrations of a laser beam and the phase of an optical wave, a linear combination of Zernike polynomials can be used. Each Zernike polynomial describes a specific aberration. The coefficients in front of the individual Zernike polynomials represent the amplitude and sign of the aberration.

Zernike polynomials are, especially for higher orders, described in a simpler form if polar coordinates instead of Cartesian coordinates are used. The Zernike polynomials in polar coordinates are given by

$$Z_n^m(\rho, \theta) = \begin{cases} R_n^m(\rho)\cos(m \cdot \theta), & \text{if } m \geq 0 \\ R_n^m(\rho)\sin(|m| \cdot \theta), & \text{if } m < 0 \end{cases} \tag{2.12}$$

with the radial polynomial $R_n^m(\rho)$ defined as

$$R_n^m(\rho) = \sum_{k=0}^{\frac{n-|m|}{2}} \frac{(-1)^k (n-k)!}{k! \left(\frac{n+|m|}{2} - k\right)! \left(\frac{n-|m|}{2} - k\right)!} \rho^{n-2k} \tag{2.13}$$

with the radial distance ρ, the azimuthal angle θ and the integers for the radial order n and the angular frequency m. $n - |m|$ can never be odd because for a given n, m can take the value of any integer from $-n$ to n but has to have the same parity as n.

The values of the Zernike polynomials are always between -1 and 1. Zernike polynomials are continuous and orthogonal over a unit circle[29] and due to their completeness[30] they can be used to represent any circular phase distribution. The Zernike polynomials in polar coordinates up to the radial order $n = 4$ are shown in Table 2.1.

The first three Zernike polynomials do not describe real aberrations. Piston just leads to an addition or subtraction of a constant phase across the entire wavefront. Vertical and horizontal tilt lead to a tilt of the wavefront and because the direction of propagation of a wave is normal to the wavefront, the beam travels at a different angle but has no curved wavefront.

Defocus is a radially symmetric aberration that leads to a converging or diverging beam and thus to a shift of the focal spot along the direction of propagation. Astigmatism of a beam can lead to different foci for rays that propagate in orthogonal planes. If focused with a spherical lens, astigmatism causes an elongated and broad focus and it is not possible to focus all the light into a single spot. The name coma originates from the comet-shaped image that is formed in the focal spot during the presence of this aberration.[31] Spherical aberration is an aberration that forms if a beam is focused with a spherical lens. The smallest possible focal spot is reached if for example a parabolic mirror is used to focus a flat wavefront.[15] Spherical lenses and spherical mirrors introduce spherical aberration and more complex aspheric lenses are needed to not introduce this aberration to a focused beam.[32]

Table 2.1: Zernike polynomials up to the radial order n=4 and their corresponding optical aberrations

Zernike Indices		Zernike Polynomials	Aberration
n	m		
0	0	$Z_0^0(\rho) = 1$	Piston
1	−1	$Z_1^{-1}(\rho) = \rho \cdot \sin(\varphi)$	Vertical Tilt
1	1	$Z_1^1(\rho) = \rho \cdot \cos(\varphi)$	Horizontal Tilt
2	−2	$Z_2^{-2}(\rho) = \rho^2 \cdot \sin(2 \cdot \varphi)$	Oblique Astigmatism
2	0	$Z_2^0(\rho) = 2\rho^2 - 1$	Defocus
2	2	$Z_2^2(\rho) = \rho^2 \cdot \cos(2 \cdot \varphi)$	Vertical Astigmatism
3	−3	$Z_3^{-3}(\rho) = \rho^3 \cdot \sin(3 \cdot \varphi)$	Vertical Trefoil
3	−1	$Z_3^{-1}(\rho) = (3\rho^3 - 2\rho) \cdot \sin(\varphi)$	Vertical Coma
3	1	$Z_3^1(\rho) = (3\rho^3 - 2\rho) \cdot \cos(\varphi)$	Horizontal Coma
3	3	$Z_3^3(\rho) = \rho^3 \cdot \cos(3 \cdot \varphi)$	Oblique Trefoil
4	−4	$Z_4^{-4}(\rho) = \rho^4 \cdot \sin(4 \cdot \varphi)$	Oblique Tetrafoil
4	−2	$Z_4^{-2}(\rho) = (4\rho^4 - 3\rho^2) \cdot \sin(2 \cdot \varphi)$	Secondary Oblique Astigmatism
4	0	$Z_4^0(\rho) = 6\rho^4 - 6\rho^2 + 1$	Primary Spherical
4	2	$Z_4^2(\rho) = (4\rho^4 - 3\rho^2) \cdot \cos(2 \cdot \varphi)$	Secondary Vertical Astigmatism
4	4	$Z_4^4(\rho) = \rho^4 \cdot \cos(4 \cdot \varphi)$	Vertical Tetrafoil

A graphical illustration of the Zernike polynomials up to the radial order $n = 4$ is depicted in Figure 2.4. The Zernike polynomials can be multiplied with a factor to span a different range than between -1 and 1 to represent the phase across the beam profile. It can be seen that piston leads to the same addition or subtraction of phase independent of the position on the beam profile. If a beam is reflected by an orthogonal mirror, then the movement of the mirror along the direction of the beam propagation introduces a different amount of piston but no aberrations. If a mirror is rotated or tilted slightly, then the phase of the beam changes in the same way as described by the Zernike polynomials corresponding to horizontal tilt or vertical tilt, respectively. It can also be seen that the Zernike polynomial corresponding to defocus describes a radially symmetric curvature of the wavefront and that will result in a converging or diverging beam. The different foci for rays propagating in two orthogonal planes in the case of astigmatism can be imagined from the orthogonally opposite curvature in the corresponding shown Zernike polynomials. The correspondence between higher order aberrations and their Zernike polynomials is more complex and harder to illustrate by simple terms.
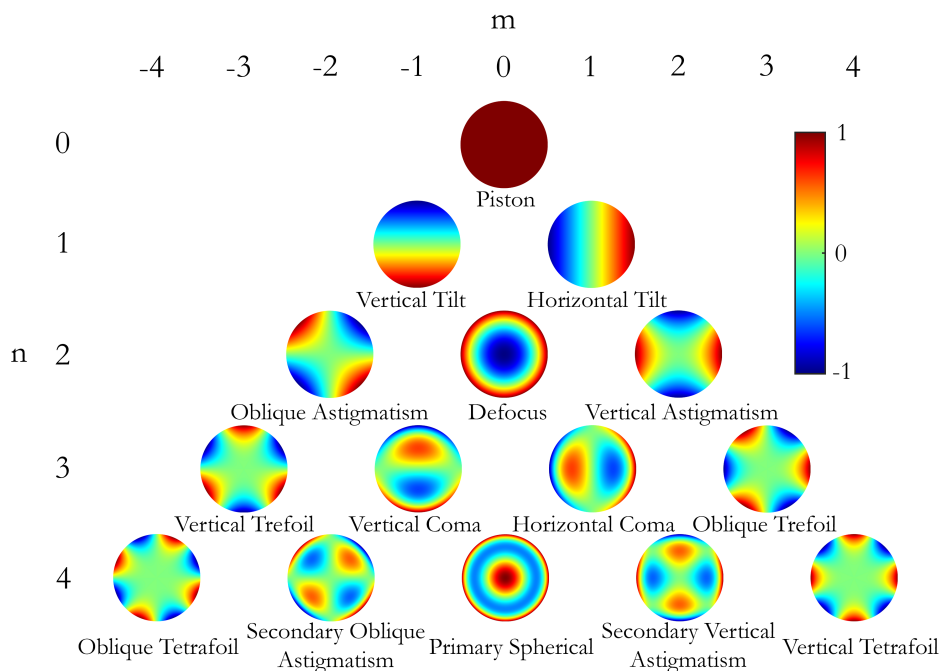

Figure 2.4: Graphical illustration of the Zernike polynomials up to the radial order $n = 4$

2.4 Phase Retrieval

To be able to correct aberrations of a laser beam with adaptive optics, the aberrations of the wavefront first have to be determined. A wavefront represents the surface with an equal phase and therefore the phase first has to be measured along the two-dimensional beam profile before aberrations can be corrected. It is not trivial to measure the phase of an optical beam and the methods usually rely on an intensity measurement in some way. The standard approach is to use a Shack–Hartmann wavefront sensor. An alternative that is used for most measurements during this project are phase retrieval algorithms.

2.4.1 Shack–Hartmann Wavefront Sensor

The Shack–Hartmann wavefront sensor was developed by Roland Shack to measure the atmospheric aberrations for the observation of satellites with ground-based telescopes and is based on the principle of the Hartmann screen test.[33] A Shack–Hartmann wavefront sensor in conjunction with a software is a direct way to measure the curvature of wavefronts at the position where the Shack–Hartmann Wavefront sensor is placed. A two-dimensional schematic representation of a Shack–Hartmann Wavefront sensor is shown in Figure 2.5.
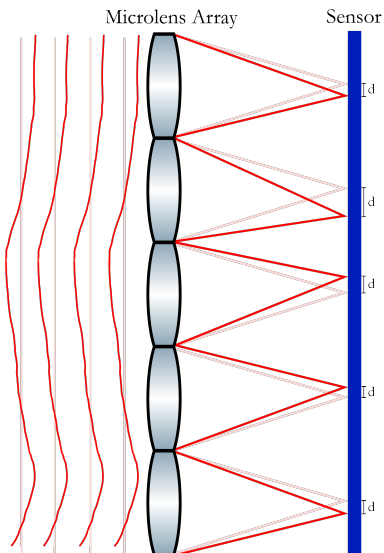

Figure 2.6: Recorded image of a wavefront measurement of the terawatt laser by a Schack-Hartmann wavefront sensor

Figure 2.5: Two-dimensional schematic representation of a Schack-Hartmann wavefront sensor

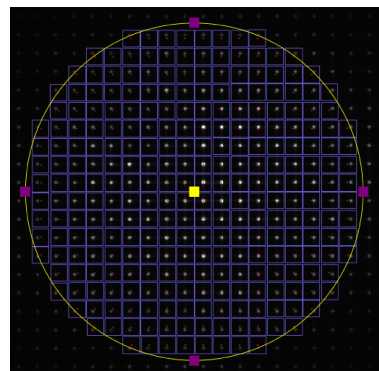A Shack–Hartmann Wavefront sensor is basically constructed out of two elements, a microlens array and a camera.[34] The microlens array is an array out of many small lenses or lenslets. Each lenslet focuses a small part of the beam onto the sensor of a camera. Depending on the curvature of the wavefront at the position of the lenslet, the focal spot appears at a different position of the sensor. For a flat wavefront, the positions of the focal spots on the sensor are known. A curved wavefront shifts the focal spot of each lenslet by a distance d on the sensor as shown in Figure 2.5. Multiple focal spots of a two-dimensional microlens array are shown in Figure 2.6. The distance and direction of the shift from the positions of the focal spots of an unaberrated beam with a flat wavefront are used by the software of the Shack–Hartmann wavefront sensor to calculate the phase map of the beam.

2.4.2 Phase Retrieval Algorithm

The complex amplitude describes a wave completely and consists out of the amplitude and the phase of the wave. The absolute value of the amplitude can easily be obtained by measuring the intensity with for example a camera and taking the square root of the measured intensity. The phase is seemingly lost when just the intensity is measured which is known as the phase retrieval problem.[35]

The Gerchberg-Saxton algorithm is an algorithm that was developed by R.W. Gerchberg and W.O. Saxton to determine the phase of electromagnetic waves from known intensities in the far field and focal plane.[36] The algorithm relies on the conditions that the two planes with the known intensities are transverse to the direction of the beam propagation and that the planes are related by a Fourier transform. The Gerchberg-Saxton algorithm can then iteratively determine the phase of the wave.

If for example the optical phase of a laser beam should be retrieved by the Gerchberg-Saxton Algorithm, then the intensities in the two planes that are Fourier transform related first have to be determined. This can be done by focusing the beam with for example a lens and by capturing one image in the far field before the lens and another image in the focal plane of the lens. The square roots of the measured intensities are proportional to the amplitudes of the beam in those two planes.

If the amplitudes are known, then the Gerchberg-Saxton algorithm is used to determine the missing phase according to the following procedure for one iteration of the Gerchberg-Saxton algorithm.

1. The amplitude in the far field A_{FF} is known due to the intensity measurement and a first guess has to be made for the phase. This guess Φ_1 can be completely random typically within the range from $-\pi$ to π or be guessed according to the expected wavefront curvature. The amplitude and the first phase guess then lead to the initial description of the field in the far field.

$$U_{FF}(x,y) = |A_{FF}(x,y)| \cdot e^{i\Phi_1(x,y)} \tag{2.14}$$

2. Now a Fourier transform of the field in the far field is performed to calculate the complex amplitude of the field in the focal plane. The calculated complex amplitude in the focal plane is then

$$U_{Focus}(x',y') = \mathscr{F}\left[|A_{FF}(x,y)| \cdot e^{i\Phi_1(x,y)}\right] = |A'_{Focus}(x',y')| \cdot e^{i\Phi_2(x',y')} \tag{2.15}$$

with the new calculated phase Φ_2 and the calculated amplitude in the focal plane A'_{Focus} that can now be replaced by the measured amplitude A_{Focus} to get an improved description of the field in the focal plane.

$$U_{Focus}(x',y') = |A_{Focus}(x',y')| \cdot e^{i\Phi_2(x',y')} \tag{2.16}$$

3. An inverse Fourier transform of U_{Focus} leads to a new calculated complex amplitude in the far field.

$$U_{FF}(x,y) = \mathscr{F}^{-1}\left[|A_{Focus}(x',y')| \cdot e^{i\Phi_2(x',y')}\right] = |A'_{FF}(x,y)| \cdot e^{i\Phi_3(x,y)} \tag{2.17}$$

The calculated amplitude is again replaced by the measured amplitude and leads to a new expression for the complex amplitude in the far field.

$$U_{FF}(x,y) = |A_{FF}(x,y)| \cdot e^{i\Phi_3(x,y)} \tag{2.18}$$

Equation 2.18 is similar to equation 2.14, but Φ_3 generally is a better description of the actual phase than the initial guess Φ_1. This one iteration of the Gerchberg-Saxton algorithm therefore leads to an improved description of the phase in the far field. The obtained expression for the complex amplitude in the far field U_{FF} is now used for the next iteration of the algorithm that starts with step 2. A Fourier transform is again performed to calculate the phase in the focal plane Φ_4 and the amplitude A_{Focus} is taken from the measurement. The inverse Fourier transform of that complex amplitude is again calculated to obtain the phase in the far field Φ_5 and this phase together with the measured amplitude A_{FF} construct the complex field after the second iteration of the algorithm.

The procedure can now be repeated as often as desired. The squared error of the differences between the calculated and measured amplitude after each iteration must always decrease or stay constant for each iteration.[36] The exact phase in both plains of the beam is obtained if the squared error is zero. Because the squared error can also stay constant if the algorithm gets stuck in a local minimum, the exact phase does not necessarily get determined more exactly if the algorithm is run for more iterations. This is due to the non-convexity of the algorithm.[37]

Several modifications and improvements to the standard Gerchberg-Saxton algorithm are possible. The error-reduction algorithm is a popular alternative to the standard Gerchberg-Saxton algorithm that improves the problem of stagnation during the iterations.[38] The input-output algorithm is another modified algorithm that converges even faster.[39] To prevent phase retrieval algorithms from stagnating in a local minimum, it is for example possible to perturb the phase slightly for every iteration, as it is done in the spatial phase perturbation Gerchberg-Saxton algorithm that can also be combined with other algorithms to further reduce the convergence time.[40]

The phase retrieval algorithm that is used for the retrieval of the phase in this project is based on the Gerchberg-Saxton algorithm, but uses measured amplitudes from different planes along the direction of the beam propagation. The two planes are not the far field and focal plane as in the standard Gerchberg-Saxton algorithm, but instead the amplitudes in planes around the focus are used. One plane is at a distance before the focus and the other plane is at the same distance behind the focus. A numerical propagator is used to propagate between the two planes around the geometrical focus during the iterations and after the spatial phases in the planes around the focus are determined, the propagation from one of the planes around the focus back to the far field is calculated.

Chapter 3

Methods

3.1　Simulations

To simulate the intensity distribution in the focal plane for different applied phase patterns on the SLM, simulations are performed in MATLAB. Since the used SLM is a phase-only SLM, the amplitude is not modulated when simulating the effect of the SLM. A Gaussian distribution with a beam diameter that corresponds to 74 % of the height of the active area of the SLM is used as the incident amplitude on the SLM to match best with the actual illumination of the SLM in the laboratory. An infinite radius of curvature is assumed for the incident wavefront. The uniform phase is then changed to a value between 0 and 2π for every pixel of the simulated SLM with a resolution of 1272 by 1024 discrete pixels. The simulated intensity in the far field corresponds to the intensity distribution in the focal plane of a lens and fast Fourier transforms are used for the simulations. Simulations are performed for a variety of phase patterns that correspond to Zernike polynomials that are converted to a range between 0 and 2π. MATLAB functions from the OTSLM Toolbox for Structured Light Methods are used for the generation of SLM phase patterns and the visualization in the far field. [41]

3.2　Setup

The setup that is used for all spatial light modulation experiments is built on an optical table and is shown in Figure 3.1. A HAMAMATSU X13139-9685 LCOS-SLM with a resolution of 1272 by 1024 pixels on an active area of 15.9 mm by 12.8 mm

is used for the spatial light modulation.[27] A Thorlabs CPS780S laser diode with a wavelength of 780 nm and power of 2.5 mW is used as the light source. The beam first passes through a linear polarizer. The polarizer is rotated in a way so that the linear polarized light is polarized horizontally so that the polarization is parallel to the horizontal orientation of the liquid crystal molecules of the SLM. This alignment with the liquid crystals of the SLM is important to only modulate the phase and not the amplitude and for angles of incidence greater than zero, as it is the case in this setup, it is also prescribed to only use horizontally polarized incident light in the operation manual of the SLM.[27]

The beam is then reflected from a 1 inch silver mirror at an angle of incidence of about $45°$. The mirror is used for adjustments to steer the beam into the desired direction. The beam is then impinging at normal incidence onto a telescope. The telescope is constructed by using two plano-convex lenses with focal lengths of 3 cm and 15 cm. It magnifies the beam five times to illuminate most of the active area of the SLM.

A pinhole with a diameter of 15 μm is used to spatially filter the beam. It acts as a low-pass filter and removes the higher spatial frequencies from the beam to reduce the aberrations and achieve a round beam profile.

The beam is then reflected onto the SLM by a 2 inch silver mirror. The 2 inch size of the mirror is used to avoid diffraction and to make sure that the entire beam is reflected at this $45°$ angle of incidence and to simplify the alignment. A round illumination of almost the entire active area of the SLM is achieved. The SLM then reflects the modulated light onto another 2 inch silver mirror. Because the SLM works best for normal incidence of the beam, it is tried to achieve an angle of incidence that is as small as possible. The distance from the first and second 2 inch mirror to the SLM is 145 cm and 137 cm, respectively. The second 2 inch mirror is placed as close as possible to the on the SLM incident beam. An angle of incident on the SLM of about $1.2°$ is achieved. The 2 inch size of the second 2 inch mirror is especially important during the generation of holograms because those patterns on the SLM lead to large and diverging modulated beams. Even larger or closer optics behind the SLM should be used for the generation of large holograms, but this is not the focus of this project and 2 inch at this distance are sufficient for testing holograms on the SLM and for wavefront corrections of aberrated beams.

A 2 inch plano-convex lens with a focal length of 30 cm is used to focus the light into a camera. A FLIR Grasshopper3 GS3-U3-91S6M-C camera is used for all images taken on this setup. It is a monochrome CCD camera with a Sony ICX814 sensor with a resolution of 3376 by 2704 pixels, a size of the active area of 12.5 mm by 10.0 mm and a pixel size of 3.69 μm.[42] The camera is mounted on top of a translation stage that allows precise adjustments of the camera position along the direction of the beam

propagation. This translation stage is not just helpful for finding the focal spot but also allows to take images of the beam profile up to 7.5 mm before and behind the focal plane for the phase retrieval measurements.
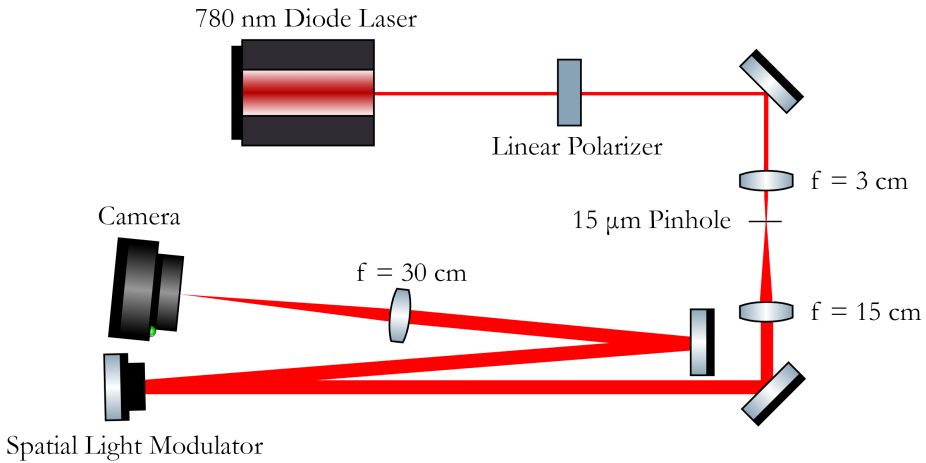

Figure 3.1: Setup that is used for all spatial light modulation experiments[1]

3.3   Programming the Spatial Light Modulator

The phase-only HAMAMATSU X13139-9685 LCOS-SLM modulates the phase of the reflected light for every pixel to a value between 0 and 2π. The active area that can be used for the modulation has a size of 15.9 mm in the horizontal direction by 12.8 mm in the vertical direction. It has a resolution of 1272 by 1024 discrete pixels that are all controlled separately by loading an integer value between 0 and 255 to each pixel. Those pixel values are then converted to a voltage on the liquid crystals that lead to a rotation of the liquid crystal molecules and a separate modulation of the phase for every pixel.

The imparted phase shift does not only depend on the orientation of the liquid crystals but also on the wavelength of the light. The employed SLM can be used for wavelengths from 750 nm to 850 nm, but the necessary voltage on the liquid crystals that is needed for a 2π phase shift changes with the wavelength. For the used 780 nm wavelength of the diode laser, a phase shift of 2π is already reached at an input signal level of 205. Therefore, just integer values between 0 and 205 are loaded to the SLM and this leads to a phase shift between 0 and 2π for the reflected beam.

---

[1]This graphic was generated with illustrations from the ComponentLibrary by Alexander Franzen [43]

Due to manufacturing imperfections and unevennesses of the surface of the SLM, a distortion correction map is always loaded on top of the desired phase map. Several correction maps for different wavelengths are provided as bitmap images by the manufacturer and the correction map for 780 nm is always added to the desired phase pattern in MATLAB.

A small percentage of the light reflected from the SLM does not get modulated because it is reflected directly from the surface of the SLM without entering the liquid crystals. Due to this zero-order reflection from the SLM, a phase pattern is also always added on top of the desired phase pattern and the correction phase pattern to shift the modulated beam to a different direction than the zero-order reflection. A linearly ramped phase pattern can be applied to the SLM to shift the zero-order reflection to a different position in the focal plane.[28] A linear tilt from 0 to 2π was applied to the SLM and led to a shift of the modulated light, but it did not lead to a complete separation from the zero-order reflection in the focal plane with this setup due to a small change of the angle of the light propagation. Instead, a phase pattern that corresponds to a linear blazed grating with a period of 0.492 mm is always added on top of the desired phase pattern and the correction phase pattern in MATLAB. The phase pattern consists out of 26 individual linear phase ramps from 0 to 2π that lead to a larger tilt of the wavefront and is shown in the middle of Figure 3.2.

(a) SLM distortion correction phase pattern   (b) Linear phase pattern   (c) Example for an applied phase pattern
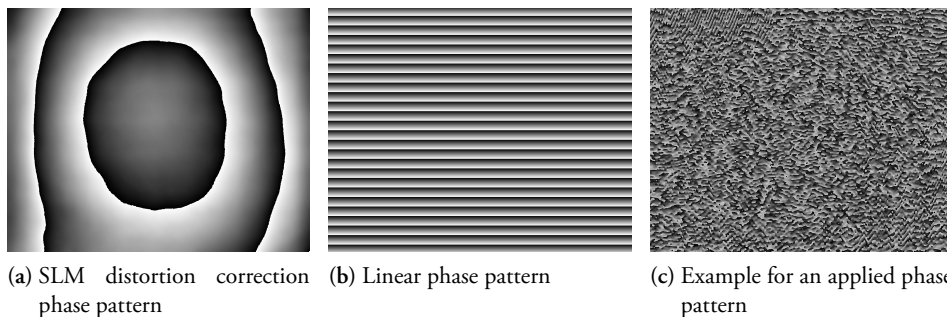
Figure 3.2: The applied phase pattern is constructed by combining the desired phase pattern, the distortion correction phase pattern for the SLM and the linear grating phase pattern

A modulo operation of the added phase patterns is performed to make sure that the uploaded pattern is always between pixel values of 0 and 205 and thus the phase shift is never larger than 2π. The remainder after division by 206 is used if the pixel values exceed 205. For example, a phase shift of 3π can not be achieved and the modulation is indistinguishable from a phase shift of π. The applied linear phase pattern leads to a slightly different angle of the reflected modulated light. The focused modulated beam thus gets shifted to a different position on the sensor of the camera.

The zero-order reflection is not altered by the phase patterns on the SLM and therefore always appears at the same position on the sensor. This allows a separation of the modulated light from the zero-order reflection and is important for just measuring the modulated light.

The SLM is configured as a second display of a PC and the phase patterns containing integer values between 0 and 205 are displayed as a BMP image in full screen mode on the second display. Due to unstable characteristics of the SLM during the warm up, the SLM was turned on at least 20 minutes before any measurements are taken.

3.3.1 Testing the SLM by Loading Linear Phase Patterns and Fresnel Lens Phase Patterns to the SLM

For initial tests of the SLM, phase patterns that correspond to blazed gratings are uploaded to the SLM. Different grating periods and different orientations of the applied phase patterns are tried and it is observed how the direction of the modulated light changes.

It is also tried to focus the beam without a lens by applying phase patterns to the SLM that resemble the phase change that a Fresnel lens would impart on the beam. Phase patterns corresponding to different focal lengths are uploaded to the SLM and the focal spot behind the SLM is determined by holding a piece of paper into the beam and looking at the paper with an infrared viewer.

3.3.2 Generating Holograms with the SLM

Due to the Fourier relation, the phase pattern in the far field contains the information for the intensity distribution in the focal plane. If a phase pattern as the one that is shown on the right hand side of Figure 3.2 is applied to the SLM, a two-dimensional hologram appears in the focal plane. To further test the SLM and to make sure that the applied phase patterns have the right orientation and rotation, holograms are generated and the corresponding phase patterns are obtained by using the Gerchberg–Saxton algorithm from the OTSLM Toolbox for Structured Light Methods.[41] The algorithm iterates between the in the focal plane desired amplitude pattern that was generated beforehand as a grayscale image and the phase pattern on the SLM. 100 iterations between both planes are computed and the obtained phase pattern is then applied to the SLM. The imaged hologram in the focal plane of the lens is compared to the simulations and the right orientation and rotation of the phase patterns on the SLM that are crucial for the later corrections of aberrations are determined.

3.3.3 Loading Zernike Aberration Polynomials on the SLM

Several aberrations that can be described by Zernike polynomials were also uploaded to the SLM. The Zernike polynomials that have values between -1 and 1 are converted into a range from 0 to 2π and the size of the circular phase patterns is chosen to match the diameter of the beam. Images in the focal plane of the 2 inch lens are recorded. The measurements are compared to the simulations.

3.4 Phase Retrieval

To optimize the focal spot of a laser beam with a SLM or deformable mirror, the aberrations of the beam have to be corrected. It is thus necessary to characterize and measure the aberrations before they can be corrected with adaptive optics. A phase retrieval algorithm is used for the measurement of the aberrations. It was developed by Cord Arnold and in the master's degree project of Mattias Ammitzböll. [44]

One image of the beam profile at a short distance before the focus and one image of the beam profile at the same distance behind the focus are recorded and used as the input for the phase retrieval algorithm. The distance from the focus is used as the initial guess for the radius of curvature because it is the best guess of the phase if the images are taken at a distance from the focus that is much larger than the Rayleigh range.

Different neutral density filters for different camera positions are mounted in front of the sensor of the camera to not overexpose the recorded images and to make sure that almost the entire dynamic range of the grayscale sensor of the camera is used. The background noise in the images is removed and the images are filtered by cutting out higher-order wave numbers. All spatial frequencies that are larger than a manually adapted threshold are removed in the frequency domain. It is also zoomed into the right region of the recorded images to remove the zero-order reflection of the SLM that appears at a different position on the sensor of the camera to not affect the quality of the phase retrieval.

The phase retrieval algorithm is always run for 100 iterations and the retrieved phase in the far field is calculated as a matrix. The far field beam size is also calculated and used to scale the retrieved phase matrix to the physical dimensions. The phase retrieval algorithm also decomposes the retrieved phase into the first 10 Zernike polynomials according to the Fringe indexing scheme. [45]

3.5 Measuring the Wavefront of Aberrated Beams

For measuring the wavefront on the setup with the diode laser that is shown in Figure 3.1, images are recorded at different distances from the focal plane of a 2 inch lens with a focal length of $30\,\text{cm}$. If the initial beam diameter is assumed to be as large as the height of the active area of the SLM, then the beam waist radius of the unfocused beam is $w_0 = 6.4\,\text{mm}$ and the Rayleigh range of the unfocused beam is

$$z_R = \frac{\pi \cdot (6.4\,\text{mm})^2}{780\,\text{nm}} = 164.97\,\text{m}. \tag{3.1}$$

The minimum waist radius to which the beam can be focused is described by [46]

$$w_0' = \frac{w_0}{\sqrt{1 + \left(\frac{z_R}{f}\right)^2}}. \tag{3.2}$$

The theoretical radius of the focal spot is thus

$$w_0' = \frac{6.4\,\text{mm}}{\sqrt{1 + \left(\frac{164.97\,\text{m}}{0.3\,\text{m}}\right)^2}} = 11.64\,\mu\text{m} \tag{3.3}$$

and can be used to calculate the Rayleigh range of the focused beam to

$$z_R' = \frac{\pi w_0'^2}{\lambda} = \frac{\pi \cdot (11.64\,\mu\text{m})^2}{780\,\text{nm}} = 545.7\,\mu\text{m}. \tag{3.4}$$

It should therefore not be attempted to record the images at distances from the focus that are not significantly larger than $545.7\,\mu\text{m}$.

Images are recorded by moving the camera on the translation stage along the beam by rotating a micrometer screw. Different distances from the focus between $1.25\,\text{mm}$ and the maximum range of the translation stage of $7.5\,\text{mm}$ are tried and the ideal distance for best results with the phase retrieval algorithm is determined experimentally. It is not trivial to know which results from the phase retrieval algorithm are better than others, but if an unaberrated beam with a flat wavefront is assumed as the incident beam on the SLM, then the ideal retrieval of the phase is the same as the applied phase pattern on the SLM. Therefore, Zernike polynomial phase patterns are applied to the SLM to introduce known aberrations to the beam. Images are then recorded at different camera positions and the retrieved phase is compared for images taken at different distances from the focus. Seven individual Zernike polynomials and one linear combination of multiple Zernike polynomials are applied to the SLM. The retrieved phase is shown as an interpolated matrix of the retrieved phase matrix in the far field and also as a phase pattern that is obtained by linearly combining the retrieved Zernike polynomials with their corresponding amplitude.

3.6   Measuring the Wavefront of the Terawatt Laser

The beamline for high-order harmonic generation at the Lund High-Power Laser Facility up to the generation chamber is depicted in Figure 3.3. The beam that is generated in another room by the terawatt laser has a repetition rate of 10 Hz and pulse energy up to 1.5 J at a center wavelength of 810 nm. 200 mJ are guided to the laboratory in vacuum in transport tubes. The pulses then get compressed in the compressor chamber down to a pulse duration of about 35 fs. After the compression, the beam is reflected from two mirrors before it hits the deformable mirror that is used for the correction of wavefront aberrations and for changing the focal length. The first piezoelectric actuator of the deformable mirror changes the curvature of the mirror and leads to a change in focal length along the direction of the beam propagation. The beam then gets focused by the focusing mirror and can for high-order harmonic generation be sent to a folding cross before it reaches the generation chamber where the pulses get focused into a gas cell or gas jet. The gas that is used for the generation of high-order harmonics gets released from a nozzle in pulses that are synchronized with the pulses of the infrared beam.

If the rotational stage is rotated to another angle, the beam that gets reflected by the focus mirror is not sent to the folding cross and generation chamber, but the beam can be sent out of a window of the compressor chamber to be analyzed by a Shack-Hartmann wavefront sensor.
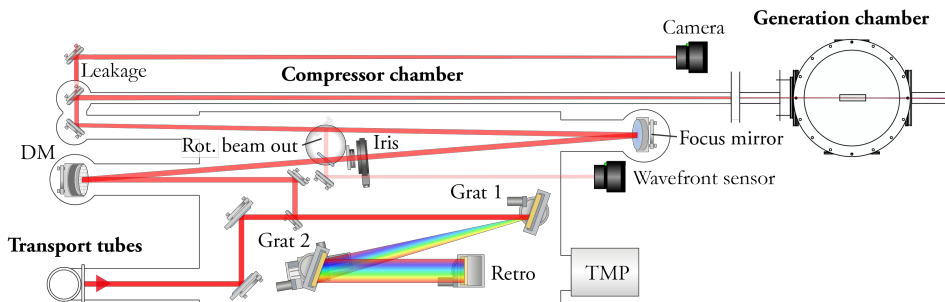
Figure 3.3: The Intense XUV Attosecond Physics beamline up to the generation chamber[2]

To characterize the aberrations of the terawatt laser, two independent methods are used. The aberrations are first measured by using a Shack-Hartmann wavefront sensor. The measured aberrations of the beam are displayed by using Zernike Polynomials. A voltage map on the 32 piezoelectric actuators of the deformable mirror that should have no impact on the wavefront other than focusing the beam is loaded for an initial

---

[2]Adapted from an unpublished graphic by Marius Plach

characterization of the aberrations. It is then attempted to optimize the wavefront by loading a different voltage map to the piezoelectric actuators of the deformable mirror. This correction map is obtained by running a hill climbing algorithm on the *Closed-loop 10.0* software by the manufacturer of the deformable mirror and Shack-Hartmann wavefront sensor.

For the characterization of the aberrations with the phase retrieval algorithm, images before and behind the focus are taken with a DAHENG IMAGING MER2-160-75GM-P camera. For this, the leakage from the last mirror before the generation chamber exits the vacuum through a window and is sent along the beamline in parallel to the beam that is used for the generation of high-order harmonics. Due to the additional path length of the leakage compared to the beam that is sent to the generation chamber, the focal spot of the leakage is reached before the generation chamber and allows to take images at different distances before and behind the focus. Due to difficulties of finding the focal spot exactly for this beam with a long Rayleigh range, images are taken at an interval of 5 cm over a range of 140 cm. Those measurements are performed for both the map on the deformable mirror that should have no impact on the wavefront other than focusing the beam and also the correction map from the measurements with the Shack-Hartmann wavefront sensor. The independent measurements from the Shack-Hartmann wavefront sensor and the retrieved phase from the images taken for the phase retrieval algorithm can then be compared.

3.7 Optimizing the Focal Spot

To optimize the focal spot on the setup with the diode laser by the SLM, the phase is retrieved with the phase retrieval algorithm as described in section 3.4. Images are taken 5 mm before and behind the estimated focal spot due to best results in previous experiments. The retrieved phase is obtained as a matrix that contains the phase for a two-dimensional region in the far field. The center region of the retrieved intensity of the beam in the far field is taken as the center of the retrieved phase. The dimensions of an extrapolated matrix of the phase correspond to the size of the active area of the SLM. The extrapolated matrix has the same resolution as the SLM. The correction pattern that can be applied to the SLM to correct the aberrations is the negative of the retrieved extrapolated matrix that is converted into a range from 0 to 2π.

An alternative approach to obtain a correction phase pattern is by using Zernike polynomials. The retrieved aberrations are expressed by using a linear combination of Zernike polynomials from order 3 up to 10 according to the Fringe indexing scheme.[45] The negative of the retrieved aberrations expressed by those Zernike polynomials are converted into a range from 0 to 2π and a correction phase pattern with

the resolution of the SLM is generated. The lower order Zernike polynomials corresponding to piston and horizontal and vertical tilt are not used because they do not correlate to aberrations. Because the beam diameter is magnified by the telescope so that it has the same height as the active area of the SLM, the size of the Zernike polynomials used for the correction phase pattern is also chosen to match the height of the active area of the SLM.

To show that the obtained correction patterns can be used to optimize the focal spot if aberrations are present, aberrations are first introduced by the SLM. Zernike polynomials up to $n = 3$ as well as a linear combination of multiple Zernike polynomials are applied separately to the SLM and the by the phase retrieval algorithm obtained correction patterns are applied on top of the originally applied patterns. This is done for both the correction pattern that is obtained from the extrapolated far field matrix as well as the correction pattern using Zernike polynomials for all 7 separately applied Zernike phase patterns and the linear combination of multiple Zernike polynomials.

To quantify the peak intensity of the focal spot, images are recorded in the focal plane and the measured peak intensity is normalized to the measured peak intensity of the focal spot of the unaberrated beam. For the measurements of the unaberrated beam, no aberrations are introduced with the SLM and just the correction pattern and linear phase pattern are applied to the SLM. The aberrations corresponding to Zernike polynomials are introduced with the SLM and the uncorrected peak intensity is measured. It is then corrected by applying the interpolated correction matrix on top of the aberration phase pattern and the peak intensity is measured again. The same procedure is done for the Zernike correction patterns.

Another approach to characterize the focal spot is by determining the full width at half maximum (FWHM) of the focused beam profile. It describes the diameter of the beam in the range for which the intensity is at least half of the peak intensity. A Gaussian curve is fitted to two perpendicular axes of the beam profile and the average of those two determined widths of the beam is taken as the FWHM of the focal spot. The determined FWHM for all the measurements are normalized to the FWHM of the focal spot for the beam without any introduced aberrations.

Even though the applied Zernike phase patterns were chosen because they correspond to realistic aberrations in optical systems, it is also attempted to correct aberrations that were not first introduced by the SLM. A phase pattern that just contains the correction pattern and the linear phase pattern is applied to the SLM to not introduce any aberrations. The 2 inch lens with a focal length of 30 cm is tilted by approximately $10°$ to introduce typical aberrations in misaligned optical setups. Correction patterns with and without using Zernike polynomials are generated by measuring 5 mm before and behind the new and slightly shifted estimated focal spot. The peak intensities and

widths of the corrected focal spots are then compared to those of the uncorrected focal spot.

At the end it is also attempted to improve the focal spot of the nearly unaberrated beam. The phase pattern that just contains the correction pattern and the linear phase pattern is again applied to the SLM and the 2 inch lens is rotated back to the previous position perpendicular to the direction of the beam propagation to not introduce any aberrations. Measurements 5 mm before and behind the focal spot are recorded and the by the phase retrieval algorithm recovered correction phase patterns with and without using Zernike polynomials are applied to the SLM to attempt to optimize the nearly unaberrated focal spot.

Chapter 4

Results and Discussion

4.1 Applying Phase Patterns to the SLM

4.1.1 Shifting and Focusing the Beam with the SLM

The application of phase patterns that correspond to blazed gratings yield the expected results. It is possible to diffract the beam into different directions and the direction of the shift of the beam depends on the orientation of the blazed grating. The diffraction angle changes for different grating periods of the applied phase pattern. The application of a phase pattern with a single ramp from 0 to 2π leads to a very small change of the angle of the modulated light. Smaller grating periods between the individual 0 to 2π phase ramps of the blazed grating phase pattern lead to larger shifts of the angle of the diffracted light from the optical axis.

The application of phase patterns that resemble the phase change that a Fresnel lens would impart on the beam also leads to the expected results. The beam is focused at distances behind the SLM that correspond to the focal length of the applied Fresnel lens phase patterns. Due to the small angle between the incident beam on the SLM and the reflected beam it is not possible to observe a focal spot for Fresnel lens phase patterns that correspond to a focal length of less than about 10 cm because the paper on which the focal spot is observed with the infrared viewer then blocks the incident beam.

4.1.2 Holograms

To further test the SLM and also to compare the orientation and rotation of the recorded images in the focal plane with the simulations, phase patterns that correspond to holograms are applied to the SLM. Images are then taken in the focal plane of the 2 inch lens with a focal length of 30 cm. Different holograms and phase patterns that lead to different sizes of the observed holograms are tried. Larger holograms lead to a higher resolution of the holograms in the focal plane, but the size of the holograms is limited by the size of the used 2 inch optics behind the SLM because the edges of large holograms correspond to large diffraction angles from the SLM and that light does not hit the mirror behind the SLM or the focusing lens if the hologram is too large. An example for a hologram that is too large can be seen in Figure 4.1 and compared to the uncut hologram on the left in Figure 4.2. The edges on the bottom left and right in the image are not reflected onto the image sensor due to the limited size of the optics. Larger holograms also have a lower brightness because the intensity is reduced if the same power of the diode laser is distributed over a larger area.
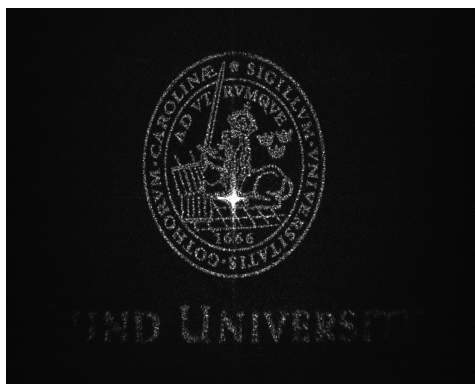
Figure 4.1: A hologram that is too large for the used setup

4.1.3 Shifting the Modulated Light away from the Zero-Order Reflection

The zero-order reflection from the SLM is the bright spot with the diffraction spikes in the middle of the images in Figure 4.1 and Figure 4.2. It always appears at the same position on the image sensor of the camera. A blazed grating phase pattern that is applied to the SLM will shift the reflected light into different angles and the by the SLM modulated beam appears at a different position on the image sensor relative to the zero-order reflection. This effect of the for all later experiments used blazed grating phase pattern with a period of 0.492 mm is shown in Figure 4.2.
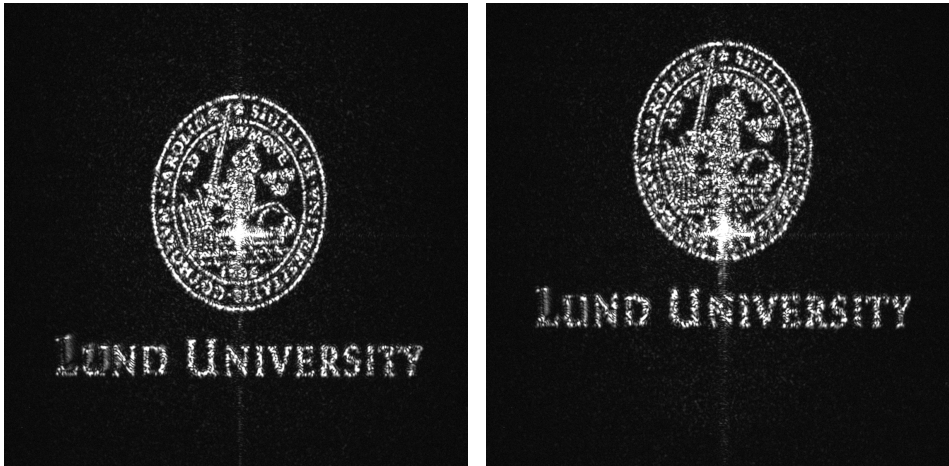
(a) Without applied linear phase pattern   (b) With applied linear phase pattern
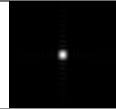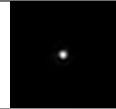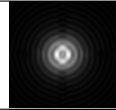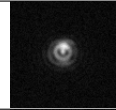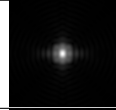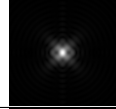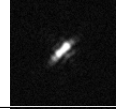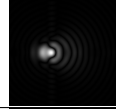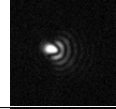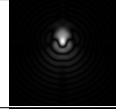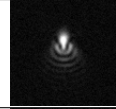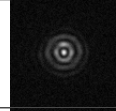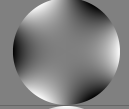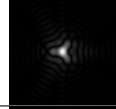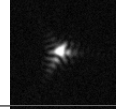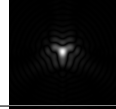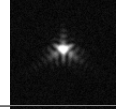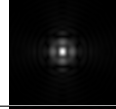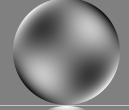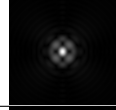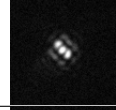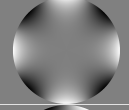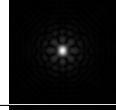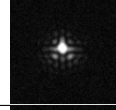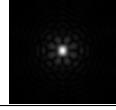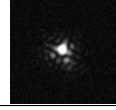
Figure 4.2: Shifting the modulated beam away from the zero-order reflection

The zero-order reflection still appears at the same position on the image sensor, but the modulated light is shifted to a different position on the image sensor which allows to separate the modulated light from the zero-order reflection in the focal plane for all later experiments. The zero-order reflection is also shifted away enough for all images taken before and behind the focus to not influence the phase retrieval algorithm by including unmodulated light.

4.1.4 Zernike Aberration Polynomials

The simulations and measurements of the aberrations in the focal plane that are introduced by applying Zernike polynomials to the SLM are shown in Table 4.1. The depicted bitmap phase patterns that correspond to phase shifts between 0 and 2π are used for the simulations and the same patterns plus the correction pattern and blazed grating phase pattern are uploaded to the SLM. The zero-order reflection is visible below the depicted region of the measured focal plane and not considered anymore because it does not affect the region of interest in the images. The measurements generally agree very well with the simulations and it is apparent that it is possible to introduce aberrations to the beam by applying Zernike polynomials to the SLM. Because an unaberrated wavefront is used for the simulations and the deviations of the measured images from the simulations are very small, it can be concluded that the aberrations of the beam before the modulation by the SLM have to be rather small.

Table 4.1: Applied phase patterns on the SLM and the intensity in the focal plane

Zernike Indices		Aberration	Phase Pattern	Simulation	Measurement
n	m				
0	0	Unaberrated			
2	0	Defocus			
2	2	Vertical Astigmatism			
2	−2	Oblique Astigmatism			
3	1	Horizontal Coma			
3	−1	Vertical Coma			
4	0	Primary Spherical			
3	3	Oblique Trefoil			
3	−3	Vertical Trefoil			
4	2	Secondary Vertical Astigmatism			
4	−2	Secondary Oblique Astigmatism			
4	4	Vertical Tetrafoil			
4	−4	Oblique Tetrafoil			

4.2 Retrieving the Wavefront of Aberrated Beams

A typical development of the integrated mean-squared error of the differences between the calculated and measured amplitude after each iteration of the phase retrieval algorithm is shown in Figure 4.3. The integrated mean-squared error drops quickly during the first 10 iterations of the algorithm. The reduction of this error after more than 100 iterations is typically very small and the computation of 100 iterations already takes a few minutes. Therefore, the phase retrieval algorithm is always run for 100 iterations for all measurements.
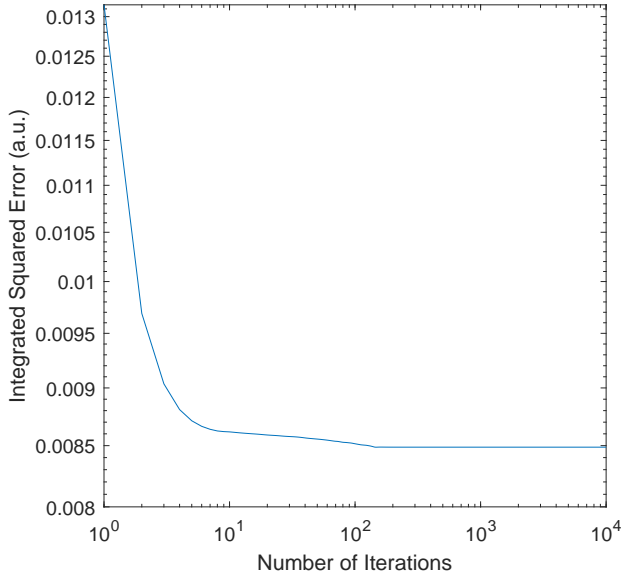
Figure 4.3: Example for the reduction of the integrated mean-square error as a function of the number of iterations for 10000 iterations of the algorithm for the measurement of the introduced aberration of oblique trefoil

The results from the phase retrieval algorithm of the by the SLM introduced aberrations yield similar retrieved phase patterns to the applied phase patterns for all tried recording distances between 1.25 mm and 7.5 mm before and behind the focus. The best results are obtained for images that are recorded 5 mm before and behind the focus. Those results are shown in Table 4.2. The position of the focal spot can be determined to an accuracy of about $500\,\mu$m with the camera on the translation stage and leads to larger relative uncertainties for small recording distances from the focus. Due to the superiority of the recording distance from the focus of 5 mm, all future images for the phase retrieval algorithm on this setup are recorded at this distance.

The applied and retrieved amplitudes of the Zernike polynomials are shown in the appendix. The results in Table 4.2 clearly show that it is possible to retrieve the aberrations of the beam with the phase retrieval algorithm. The phase patterns are shown for the same size as the size of the active area of the SLM. All applied phase patterns on the SLM can be reconstructed to a high visual similarity. The directly retrieved interpolated phase maps look noisy compared to the applied phase patterns, but the size and amplitude of the retrieved phase patterns generally matches the applied patterns very well. Smoother and less noisy looking retrieved phase patterns are obtained if the retrieved Zernike polynomials of the aberrations are used to construct the images. The size of the Zernike polynomials is selected to match the beam diameter and have the same height as the active area of the SLM because this corresponds very well to the size of the directly retrieved phase patterns in the far field as shown in Table 4.2.

Table 4.2: Applied phase patterns on the SLM and the retrieved phase patterns with and without using Zernike polynomials

Zernike Indices		Aberration	Applied	Retrieved	Retrieved Zernike
n	m				
2	0	Defocus			
2	2	Vertical Astigmatism			
2	−2	Oblique Astigmatism			
3	1	Horizontal Coma			
3	−1	Vertical Coma			
3	3	Oblique Trefoil			
3	−3	Vertical Trefoil			

Phase (rad)
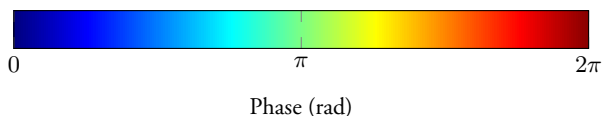
The linear combination of multiple Zernike polynomials that is applied to the SLM is constructed by combining 0.5 times the Zernike polynomial corresponding to oblique astigmatism plus 0.3 times horizontal coma plus 0.2 times vertical astigmatism and is shown on the left in Figure 4.5. The amplitudes of the retrieved decomposed aberrations are shown as the coefficient of the individual Zernike polynomials in Figure 4.4. The coefficients of the individual Zernike polynomials are not recovered completely and the amplitudes of the decomposed aberrations deviate from the applied amplitudes by up to a value of 0.174 in the case of oblique astigmatism.
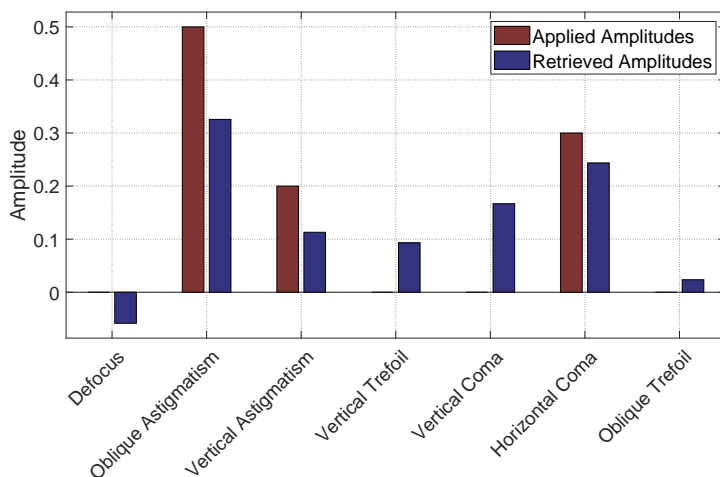
Figure 4.4: Amplitudes of the applied aberrations and the retrieved aberrations as the coefficient of the decomposed individual Zernike polynomials for the applied phase pattern constructed from a linear combination of multiple Zernike polynomials

The directly retrieved interpolated phase pattern is shown in the middle of Figure 4.5 and the by the retrieved Zernike polynomials reconstructed phase pattern is shown on the right-hand side of Figure 4.5. The retrieved phase patterns confirm the results from the experiments with the individually applied Zernike phase patterns. The retrieved aberrations without Zernike polynomials match the size of the applied phase pattern very well but the noisy looking image does not look completely similar to the applied phase pattern. Despite the deviations of the retrieved amplitudes of the Zernike polynomials shown in Figure 4.4, the phase pattern that is obtained from the retrieved Zernike polynomials and shown on the right hand side of Figure 4.5 does appear vastly similar to the applied phase pattern on the left of Figure 4.5.

(a) Applied phase pattern

(b) Retrieved phase pattern

(c) Retrieved Zernike phase pattern
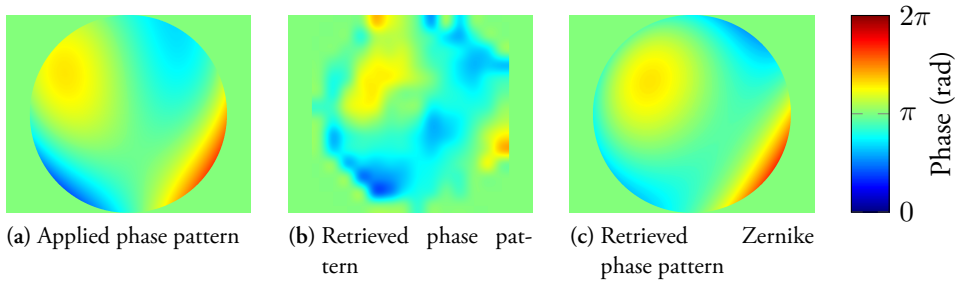
Figure 4.5: Applied phase pattern that is a linear combination of Zernike polynomials and the by the phase retrieval algorithm retrieved phase patterns

The results from the retrieval of the phase patterns that are applied to the SLM show that applied Zernike polynomials can be recovered very well if the retrieved Zernike polynomials are used for the generation of the retrieved phase patterns. The directly retrieved phase patterns without using Zernike polynomials give a lower visual similarity to the applied phase patterns. At this point it is not absolutely certain that the Zernike polynomials give the better retrieved aberrations for applied Zernike phase patterns because it is also possible that the almost aberration-free incident beam already has small higher order aberrations that can not be described by the first ten orders of Zernike polynomials or that further aberrations are introduced to the beam behind the SLM that might also not be described so well by the first ten orders of Zernike polynomials. It is therefore important to use and compare both methods for the correction of aberrations in later experiments to verify that the first ten orders of Zernike polynomials give a better description of the actual aberrations of the beam and that the phase patterns without Zernike polynomials just contain random noise.

4.3 Characterization of the Terawatt Laser

Figure 4.6 shows the measurement of the wavefront of the terawatt laser by using the Shack-Hartmann wavefront sensor. The first 20 Zernike Polynomials according to the Fringe indexing scheme[45] without the first 4 polynomials are used to show the aberrations of the beam. The aberrations that are shown on the left were measured for a voltage map on the actuators of the deformable mirror that should have no impact on the wavefront other than focusing the beam. Although those aberrations are rather small with an average root mean square deviation of $0.0744\,\mathrm{rad}$ from a perfect wavefront, the purpose of the deformable mirror is to correct those aberrations.

A hill climbing algorithm was run with the software of the wavefront sensor and the deformable mirror to correct the aberrations of the beam by applying a voltage map to the electrodes of the piezoceramic material to deform the reflective surface of the deformable mirror. The corrected wavefront of the terawatt laser is shown on the right hand side of Figure 4.6 and shows that the deformable mirror does improve the wavefront and the deviations from a perfect wavefront with this voltage map are reduced to a root mean square error of 0.0330 rad. The improvements to the beam quality are significant, but unfortunately smaller aberrations remain and the reasons for this are unclear. It could be attributed to a number of factors ranging from imperfect wavefront sensing or the possibility that the aberrations are not suited for correction using the chosen deformable mirror to inherent limitations of the software employed in adjusting the actuators of the deformable mirror.

(a) Phase pattern of the beam for the no impact map on the deformable mirror

(b) Phase pattern of the beam for the hill climbing optimized map on the deformable mirror
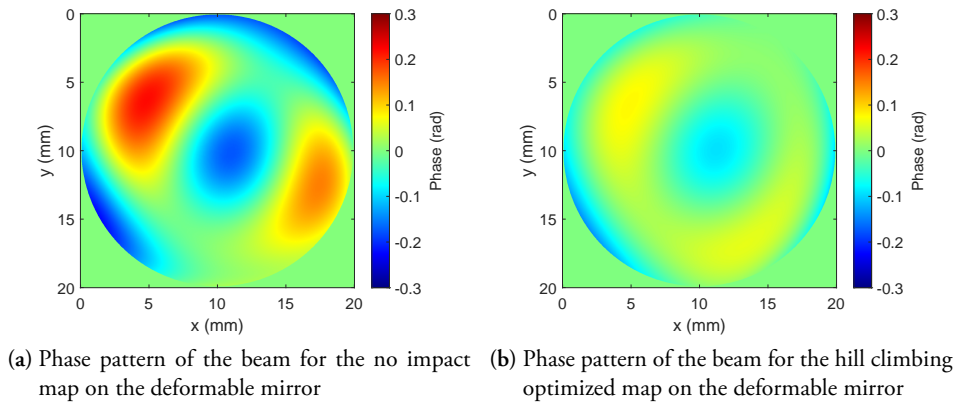
Figure 4.6: Wavefront of the terawatt laser obtained with the Shack-Hartmann wavefront sensor

To compare the measurements with the Shack-Hartmann wavefront sensor of the aberrations with an independent alternative, the taken images before and behind the focus of the leakage of the terawatt laser are used with the phase retrieval algorithm to obtain the wavefront. The position of the camera where the beam diameter is measured to be the smallest is taken as the focal spot. The distance of the camera position of 37.5 cm from this focal spot is used for the recording of the images for the phase retrieval algorithm. The use of other camera positions for the capturing of the images for the phase retrieval algorithm leads to similar results. The aberrations for both voltage maps on the deformable mirror that are directly shown as an interpolated far field phase map of the retrieved phase are depicted in Figure 4.7.
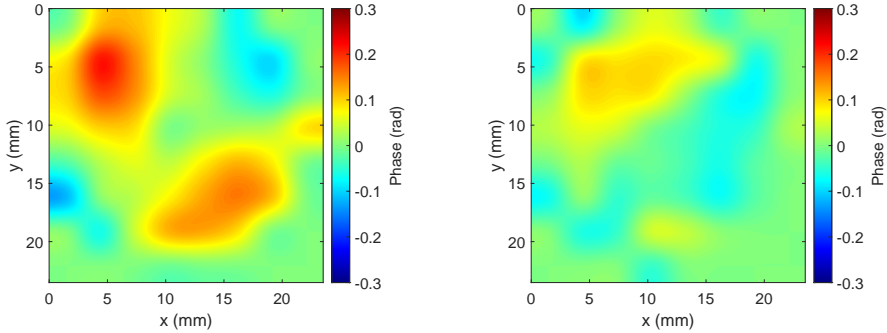
(a) Phase pattern of the beam for the no impact map on the deformable mirror

(b) Phase pattern of the beam for the hill climbing optimized map on the deformable mirror

Figure 4.7: Wavefront of the terawatt laser obtained with the phase retrieval algorithm

To better compare the retrieved phase with the results from the Shack-Hartmann wavefront sensor, the aberrations are expressed in terms of Zernike polynomials and the same size and scale as for the Shack-Hartmann wavefront sensor measurements is used. The measured aberrations are depicted in Figure 4.8 and confirm the reduction of aberrations when the optimized voltage map is applied to the deformable mirror. In particular, the RMS deviation from an unaberrated wavefront reduces from 0.0571 rad to 0.0224 rad.
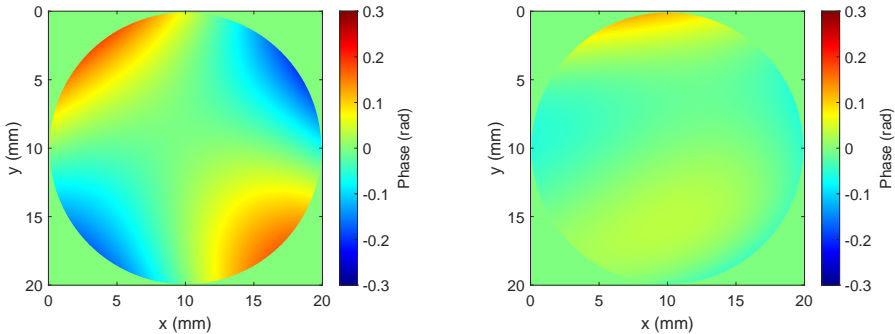
(a) Phase pattern of the beam for the no impact map on the deformable mirror

(b) Phase pattern of the beam for the hill climbing optimized map on the deformable mirror

Figure 4.8: Wavefront of the terawatt laser obtained with the phase retrieval algorithm and expressed by the first ten orders of Zernike polynomials

Even though the results from the measurements with the two independent methods do not match perfectly, the reduction of the aberrations by improvements to the wavefront by the deformable mirror are confirmed by both the Shack-Hartmann wavefront sensor and the phase retrieval algorithm to a reduction of the RMS deviations by a factor of 2.25 and 2.55, respectively.

The reason for the differences in the measured aberrations between both methods is not clear. It could be due to a change of the aberrations between the time of both measurements or measurement uncertainties with the Shack-Hartmann wavefront sensor or the phase retrieval algorithm but also due to different aberrations at the location of the Shack-Hartmann wavefront sensor and the camera that is used for the recording of the images for the phase retrieval algorithm. The focus mirror, the folding cross and the mirror that is used to send the beam leakage along the beamline can all have an impact on the wavefront that is measured with the phase retrieval algorithm but not on the measurements by the Shack-Hartmann wavefront sensor as shown in Figure 3.3. The passing of the focused beam through the substrate of a mirror of the folding cross at an angle of incidence of $45°$ will also induce some aberrations to the leakage. Future measurements on the same location of the beam with both methods would clarify the validity of this theory, but the final shutdown of the terawatt laser prevents this for now.

4.4   Focal Spot Optimization

4.4.1   Correcting Zernike Aberrations that are introduced by the SLM

The introduction of the aberrations by the SLM leads to a reduced peak intensity of the focal spot. The application of the by the phase retrieval algorithm obtained correction patterns on top of the originally applied aberration patterns increases the peak intensity again as shown in Table 4.3. All measured peak intensities of the aberrated focal spot and the by the interpolated matrix corrected peak intensity in the focal spot and the by the Zernike correction pattern corrected focal spot are all normalized to the peak intensity of the not by the SLM aberrated focal spot.

Table 4.3: Peak intensity normalized to the not by the SLM aberrated peak intensity in the focal spot

Zernike Indices		Aberration	Uncorrected	Correction Pattern	Zernike Correction
n	m				
2	0	Defocus	0.265	1.018	1.071
2	2	Vertical Astigmatism	0.465	0.969	0.978
2	−2	Oblique Astigmatism	0.460	0.836	0.942
3	1	Horizontal Coma	0.637	0.903	0.991
3	−1	Vertical Coma	0.456	0.562	0.872
3	3	Oblique Trefoil	0.518	0.845	0.912
3	−3	Vertical Trefoil	0.509	0.894	0.867

The results show that the peak intensity drops to an average value of 47.3 % of the original peak intensity if Zernike aberrations are introduced with the SLM. The correction of the aberrations with the from the phase retrieval algorithm obtained correction phase patterns on the SLM improves the focus substantially. The average peak intensity for the correction phase patterns without using Zernike polynomials increases to 86.1 % of the original peak intensity of the beam without introduced aberrations and increases the peak intensity by a factor of 1.82. The correction of the aberrations with the Zernike polynomial correction patterns yields an average peak intensity of 94.8 % of the peak intensity with no aberration phase patterns applied to the SLM and increases the peak intensity compared to the uncorrected aberrations by a factor of 2.00.

The use of Zernike polynomials for the generation of the correction phase patterns leads to better results than the use of correction phase patterns without using Zernike polynomials in all cases for the introduced aberrations except vertical trefoil. This could be due to the noise in the directly retrieved phase maps that is filtered by the decomposition into Zernike polynomials but also due to the presence of just lower order aberrations that were introduced in terms of Zernike polynomials.

It should be noted that the correction of defocus leads to higher peak intensities than the measurement of the focal spot of the not by the SLM aberrated beam. This shows that the SLM does not just manage to correct the aberrations that were introduced by the SLM, but also the aberrations that are inherent to the setup. It can thus be concluded that the incident beam is not completely aberration-free or that the initial measurement of the unaberrated focal spot was not performed exactly in the focal plane and that it should be possible to achieve an even higher peak intensity if the almost unaberrated incident beam is corrected.

As an alternative method to characterize the focal spot, the FWHM is also calculated and normalized to the FWHM of the unaberrated beam of 21.235 μm.

Table 4.4: FWHM normalized to the not by the SLM aberrated FWHM in the focal spot

Zernike Indices		Aberration	Uncorrected	Correction Pattern	Zernike Correction
n	m				
2	0	Defocus	2.490	0.905	0.921
2	2	Vertical Astigmatism	1.664	0.984	1.020
2	−2	Oblique Astigmatism	1.662	1.014	1.046
3	1	Horizontal Coma	1.132	0.978	1.047
3	−1	Vertical Coma	1.457	1.375	1.115
3	3	Oblique Trefoil	1.429	1.064	1.109
3	−3	Vertical Trefoil	1.462	1.079	1.126

The FWHM of the aberrated beams increased on average by 61.4 % compared to the focal spot without introduced aberrations. The FWHM of the focal spot for the correction patterns without using Zernike polynomials is reduced to on average just 5.69 % larger values than the FWHM of the unaberrated beam. The Zernike correction patterns reduce the FWHM of the focal spots to 5.48 % more than the focal spot of the beam without introduced aberrations. Both approaches to correct the aberrations thus lead to on average very similar results in the improvement of the width of the focal spot. The correction of vertical coma with the Zernike polynomial correction pattern leads to a much better result, but in all other cases the correction with the Zernike polynomial correction patterns performed slightly worse than the correction without using Zernike polynomials.

It is shown that the FWHM can be reduced by 34.50 % by using the retrieved correction patterns without the use of Zernike polynomials and by 34.63 % with using Zernike polynomials for the correction pattern. Even though this shows a clear reduction in beam width and improvement of the focal spot, it is not clear how well the parameter of FWHM actually describes strongly aberrated beam profiles. Gaussian curves are fitted to all beam profiles to determine the FWHM, but strongly aberrated beams do not have a Gaussian intensity distribution in the focal plane. The parameter of the peak intensity in the focal spot is independent from any assumed beam profiles and is probably a better indication of the quality of the focal spot.

4.4.2 Correcting Complex Aberrations that are introduced by the SLM

Since the individual application of Zernike polynomials to the SLM and the correction of those aberrations led to promising results, it is now attempted to apply a linear combination of multiple Zernike polynomials as an aberration phase pattern to the SLM and to correct those aberrations. The applied pattern is randomly chosen as the linear combination of 0.5 times the Zernike polynomial corresponding to oblique astigmatism plus 0.3 times horizontal coma plus 0.2 times vertical astigmatism.

By retrieving the phase and correcting the aberrations, the peak intensity could be increased and the FWHM is reduced for both applied correction phase patterns. For the correction phase pattern without using Zernike polynomials, the peak intensity compared to the aberrated beam could be increased by 17.54 % and the FWHM is reduced by 7.35 %. The correction with Zernike polynomials leads to an increase in peak intensity of 20.85 % and reduction of FWHM of 9.75 %.

4.4.3 Correcting Aberrations that are Introduced by a Tilted Lens

The tilt of the 2 inch lens leads to a shifted focal spot. The new focal spot is estimated by moving the camera to the position where the beam appears the smallest and the measured focal spot is shown on the left in Figure 4.10. The tilt around the vertical axis of the lens introduces a strong aberration of vertical astigmatism as shown in Figure 4.9.
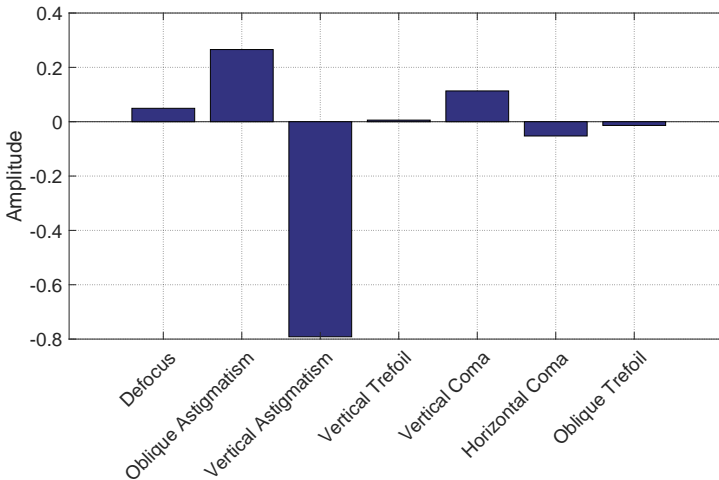

Figure 4.9: Amplitudes of the retrieved aberrations as the coefficient of the decomposed individual Zernike polynomials for the uncorrected setup with the tilted lens

The application of the retrieved correction phase pattern without the use of Zernike polynomials leads to the improved focus that is depicted in the middle of Figure 4.10. On the right-hand side of Figure 4.10, the by the retrieved Zernike correction pattern improved focal spot is shown.
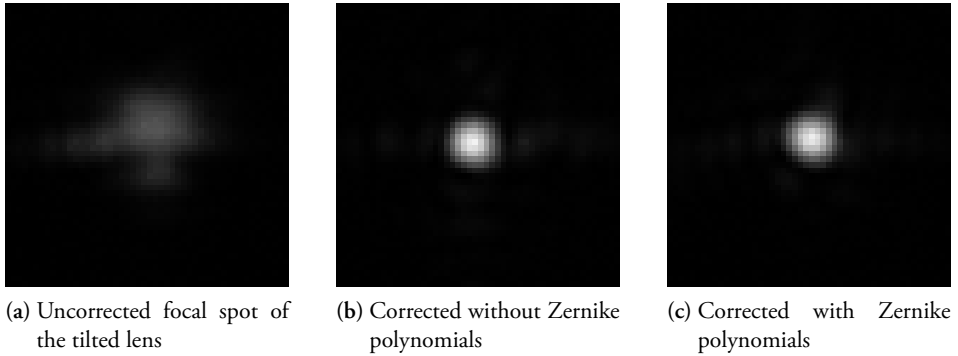

(a) Uncorrected focal spot of the tilted lens

(b) Corrected without Zernike polynomials

(c) Corrected with Zernike polynomials

Figure 4.10: Measured focal spot of the setup with the tilted lens

The same camera settings have been used for the recording of the three images. It is visually clear that the tilt of the lens introduces strong aberrations to the beam and this is confirmed by the retrieved aberrations shown in Figure 4.9. The beam profile does not look Gaussian and the peak intensity is low. Both correction patterns on the SLM improve the focal spot substantially. In particular, the correction pattern that is obtained from the interpolated retrieved phase pattern matrix in the far field increased the peak intensity by a factor of 2.85 and reduced the FWHM of previously $40.42\,\mu$m to $18.68\,\mu$m. The correction of the aberrations introduced by the tilted lens with the correction pattern with Zernike polynomials, increases the peak intensity by a factor of 2.79 and reduces the FWHM of the beam in the focus to $19.43\,\mu$m.

This results show that it is not just possible to correct simple aberrations that are introduced with the SLM, but that it is also possible to correct complex aberrations that occur in typical optical setups both with and without using Zernike polynomials for the generation of the correction phase patterns. In this example, the Zernike polynomial correction pattern performs slightly worse than the correction pattern without Zernike polynomials. This could be due to more complex aberrations that are not described so well with just the first ten orders of Zernike polynomials. Just the first ten Zernike polynomials still manage to improve the focal spot remarkably and the use of more higher order Zernike polynomials could potentially lead to even better results.

4.4.4 Correcting Aberrations that are Inherent to the Setup

The application of the phase pattern that just contains the correction pattern for the manufacturing imperfections of the SLM and the linear phase pattern leads to the nearly unaberrated focal spot that is depicted on the left in Figure 4.11. The SLM basically just reflects the light like a mirror without introducing any aberrations or corrections to the wavefront. This nearly unaberrated beam profile has previously been used for comparisons to aberrated and corrected beams. The correction of the by the SLM introduced aberration of defocus as described in section 4.4.1 led to a slightly higher peak intensity than the peak intensity of this nearly unaberrated focal spot and indicated that it should be possible to improve the focal spot of this nearly unaberrated beam either by correcting aberrations or shifting the focal spot exactly to the position of the sensor of the camera.

Even though the setup has been carefully aligned, small misalignments remain in the setup and it is possible to improve the focal spot slightly by applying the correction patterns that are obtained from the phase retrieval algorithm to the SLM. The correction with the directly retrieved phase pattern without using Zernike polynomials improves the peak intensity slightly by 2.49 % but also increases the FWHM marginally by 0.32 % and the focal spot is shown in the middle in Figure 4.11. The use of the correction pattern that is based on Zernike polynomials yields the focal spot depicted to the right-hand side of Figure 4.11. Compared to the uncorrected beam, the peak intensity is increased by 4.15 % and the FWHM decreases by 1.26 %.
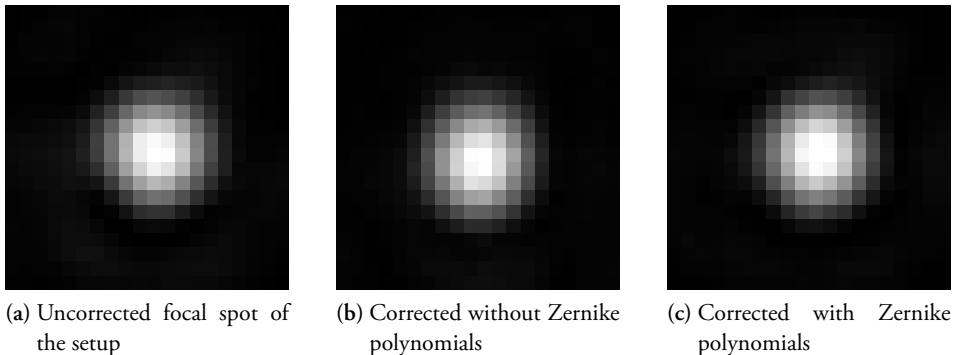

(a) Uncorrected focal spot of the setup   (b) Corrected without Zernike polynomials   (c) Corrected with Zernike polynomials

Figure 4.11: Measured focal spot of the setup without any introduced aberrations

The correction of the remaining aberrations in the well-aligned setup is hence possible but limited due to the small room for improvement of the already Gaussian looking beam profile. The use of the correction pattern with the first 10 Zernike polynomials yields the best results and indicates that the aberrations that are inherent to the setup

can be described well by using those lower order Zernike polynomials.

Chapter 5

Conclusion and Outlook

This project shows that setups containing adaptive optics can be used to improve the focal spot of a laser beam. In particular, it was shown that by capturing two images around the focus and using a phase retrieval algorithm it is possible to retrieve the phase of a laser beam in the far field and that the obtained aberrations to the wavefront can be corrected by using spatial light modulation to optimize the focal spot.

All aberrations that were introduced to the beam could be corrected very well by both applying the correction phase pattern with and without Zernike polynomials. The correction pattern that just applies a linear combination of the first ten orders of Zernike polynomials seems to mostly lead to a better correction of the aberrations than the direct use of the retrieved interpolated phase pattern without using Zernike polynomials. This is especially true for simple aberrations that were introduced by applying phase patterns corresponding to Zernike polynomials or linear combinations of Zernike polynomials to the SLM. The peak intensity increased in all cases if either of the two retrieved correction patterns was applied to the SLM, but the Zernike polynomial phase patterns led to a better description of those wavefront aberrations and to higher peak intensities of the corrected focal spots.

Complex and realistic aberrations that a misaligned and tilted lens introduces to a beam could be corrected very well by applying correction patterns with and without using Zernike polynomials to the SLM. Those experiments resulted in the only inferiority of the correction of the focal spot by using a correction pattern with Zernike polynomials. This is likely due to the complexity of the introduced aberrations that can not be described so well with just the first ten orders of Zernike polynomials. Future experiments could investigate the use of more higher order Zernike polynomials for the generation of the correction phase pattern. Those experiments would clarify

whether Zernike polynomials always lead to a better correction of realistic aberrations if the right number of Zernike polynomials are used, or if the direct correction by using the interpolated retrieved phase pattern leads to better results in certain cases. It should be noted that the use of just the first ten orders of Zernike polynomials for the generation of the correction phase pattern still leads to a considerable improvement of the focal spot and just slightly smaller improvements to the focal spot than the use of the correction pattern without Zernike polynomials.

Spatial light modulation in conjunction with this phase retrieval algorithm could be used in almost every setup to improve the focal spot. This could be shown by improving the focal spot of a well-aligned setup that already produced a nearly unaberrated focal spot before any wavefront corrections. The improvement to the focal spot are limited by the minimum spot size that can physically be obtained and the focal spot in an almost aberration-free setup can thus not be improved much.

The project shows that all aberrations on the built setup could be measured and corrected reliably. Future work should replicate this focal spot optimization with different lasers and on different setups such as the intense XUV beamline of the Lund High-Power Laser Facility. The beam size of this setup is larger than the size of the used SLM and prevents a direct implementation. If a sufficiently large SLM that can tolerate the high power of the laser would be implemented to the beamline or alternatively a software for the already used deformable mirror that can correct aberrations according to the specified Zernike polynomials of the aberrations would exist, then the phase retrieval algorithm could be used together with the adaptive optics to correct the aberrations of the beam to improve the focal spot for all future experiments on this beamline.

References

[1] Albert Einstein. Zur Quantentheorie der Strahlung. *Physikalische Zeitschrift*, 18: 121–128, 1917.

[2] Theodore Maiman. Stimulated optical radiation in ruby. *Nature*, 187:493–494, 08 1960. doi: 10.1038/187493a0.

[3] A. L. Schawlow and C. H. Townes. Infrared and optical masers. *Phys. Rev.*, 112: 1940–1949, 12 1958. doi: 10.1103/PhysRev.112.1940.

[4] Max Planck. Ueber das Gesetz der Energieverteilung im Normalspectrum. *Annalen der Physik*, 309(3):553–563, 1901. doi: 10.1002/andp.19013090310.

[5] B.E.A. Saleh, M.C. Teich. *Fundamentals of Photonics Part II: Photonics*, chapter 21: Laser Amplifiers, page 620. John Wiley & Sons, Inc., 2019. ISBN 9781119506898.

[6] B.E.A. Saleh, M.C. Teich. *Fundamentals of Photonics Part II: Photonics*, chapter 21: Laser Amplifiers, page 634. John Wiley & Sons, Inc., 2019. ISBN 9781119506898.

[7] B.E.A. Saleh, M.C. Teich. *Fundamentals of Photonics Part I: Optics*, chapter 2: Wave Optics, page 51. John Wiley & Sons, Inc., 2019. ISBN 9781119506867.

[8] B.E.A. Saleh, M.C. Teich. *Fundamentals of Photonics Part I: Optics*, chapter 3: Beam Optics, page 82. John Wiley & Sons, Inc., 2019. ISBN 9781119506867.

[9] B.E.A. Saleh, M.C. Teich. *Fundamentals of Photonics Part I: Optics*, chapter 3: Beam Optics, page 85. John Wiley & Sons, Inc., 2019. ISBN 9781119506867.

[10] Javier Alda. Laser and Gaussian Beam Propagation and Transformation. *Encyclopedia of Optical Engineering*, 01 2003.

[11] Cong Chen and Haiyan Chen. Coherence time-bandwidth product for chirped gaussian pulses. *Optik*, 124(21):5199–5201, 2013. doi: 10.1016/j.ijleo.2013.03.127.

[12] Herman A Haus. Mode-locking of lasers. *IEEE Journal of Selected Topics in Quantum Electronics*, 6(6):1173–1185, 2000.

[13] M. J. Soileau, William E. Williams, Nastaran Mansour, and Eric W. Van Stryland. Laser-induced damage and the role of self-focusing. *Optical Engineering*, 28(10):1133–1144, 10 1989. doi: 10.1117/12.7977098.

[14] Donna Strickland and Gerard Mourou. Compression of amplified chirped optical pulses. *Optics Communications*, 56(3):219–221, 1985. ISSN 0030-4018. doi: 10.1016/0030-4018(85)90120-8.

[15] Eugene Hecht. *Optics*, chapter 5: Geometrical Optics. Pearson Education, 2017. ISBN 978-1-292-09693-3.

[16] Thomas Bifano. Adaptive imaging: MEMS deformable mirrors. *Nature Photonics*, 5:21–23, 01 2011. doi: 10.1038/nphoton.2010.297.

[17] Denis Brousseau, Ermanno F. Borra, and Simon Thibault. Wavefront correction with a 37-actuator ferrofluid deformable mirror. *Opt. Express*, 15(26):18190–18199, 12 2007. doi: 10.1364/OE.15.018190.

[18] Arthur D. Fisher. Spatial Light Modulators: Functional Capabilities, Applications, and Devices. *International Journal of Optoelectronics*, 5(2):125 – 167, 05 1990.

[19] Boris Braverman, Xialin Liu, and Robert W. Boyd. How an Acousto-Optic Modulator can be used as a Spatial Light Modulator. *OSA Advanced Photonics Congress (AP) 2020 (IPR, NP, NOMA, Networks, PVLED, PSC, SPPCom, SOF)*, 2020. doi: 10.1364/PSC.2020.PsM3F.5.

[20] Masahide Okazaki, Syuhei Yoshimoto, Takao Chichibu, and Toshiaki Suhara. Electro-Optic Spatial Light Modulator Using Periodically-Poled MgO:s-LiTaO3 Waveguide. *IEEE Photonics Technology Letters*, 27(15):1646–1648, 2015. doi: 10.1109/LPT.2015.2433313.

[21] William E. Ross, Demetri Psaltis, and Robert H. Anderson. Two-Dimensional Magneto-Optic Spatial Light Modulator For Signal Processing. *Optical Engineering*, 22(4):485–490, 1983. doi: 10.1117/12.7973148.

[22] Larry J. Hornbeck. Deformable-Mirror Spatial Light Modulators. In *Spatial Light Modulators and Applications III*, volume 1150, pages 86 – 103. International Society for Optics and Photonics, 1990. doi: 10.1117/12.962188.

[23] Zichen Zhang, Zheng You, and Daping Chu. Fundamentals of phase-only liquid crystal on silicon (LCOS) devices. *Light: Science and Applications*, 3(e213), 10 2014. doi: 10.1038/lsa.2014.94.

[24] B.E.A. Saleh, M.C. Teich. *Fundamentals of Photonics Part I: Optics*, chapter 6: Polarization Optics, page 244. John Wiley & Sons, Inc., 2019. ISBN 9781119506867.

[25] B.E.A. Saleh, M.C. Teich. *Fundamentals of Photonics Part II: Photonics*, chapter 21: Electro-Optics, page 996. John Wiley & Sons, Inc., 2019. ISBN 9781119506898.

[26] B.E.A. Saleh, M.C. Teich. *Fundamentals of Photonics Part II: Photonics*, chapter 21: Electro-Optics, page 998. John Wiley & Sons, Inc., 2019. ISBN 9781119506898.

[27] HAMAMATSU. LCOS-SLM X13139 Series Operation Manual, Doc. No. K51-B60010 Revision F, 01 2018.

[28] Hao Zhang, Jinghui Xie, Juan Liu, and Yongtian Wang. Elimination of a zero-order beam induced by a pixelated spatial light modulator for holographic projection. *Applied optics*, 48(30):5834–5841, 10 2009. doi: 10.1364/AO.48.005834.

[29] Victor L. Genberg, Gregory J. Michels, and Keith B. Doyle. Orthogonality of Zernike polynomials. In *Optomechanical Design and Engineering 2002*, volume 4771, pages 276 – 286. International Society for Optics and Photonics, SPIE, 2002. doi: 10.1117/12.482169.

[30] Alfred Wünsche. Generalized Zernike or disc polynomials. *Journal of Computational and Applied Mathematics*, 174(1):135–163, 2005. ISSN 0377-0427. doi: 10.1016/j.cam.2004.04.004.

[31] Alex Small. Spherical aberration, coma, and the Abbe sine condition for physicists who don't design lenses. *American Journal of Physics*, 86(7):487–494, 07 2018. doi: 10.1119/1.5036939.

[32] Edmund Optics. All about aspheric lenses. `https://www.edmundoptics.eu/knowledge-center/application-notes/optics/all-about-aspheric-lenses/`. Accessed: 2023-06-01.

[33] Jim Schwiegerling and Daniel R. Neal. Historical Development of the Shack-Hartmann Wavefront Sensor. 01 2005. URL `https://www.lumetrics.com/hubfs/Lumetrics_August2021/PDF/Historical-Development.pdf`. Accessed: 2023-06-01.

[34] Daniel R. Neal, James Copland, and David A. Neal. Shack-Hartmann wavefront sensor precision and accuracy. volume 4779, pages 148–160, 09 2002. doi: 10.1117/12.450850.

[35] L. S. Taylor. The phase retrieval problem. *IEEE Transactions on Antennas and Propagation*, 29:386–391, 03 1981. doi: 10.1109/TAP.1981.1142559.

[36] R.W. Gerchberg, W.O. Saxton. A Practical Algorithm for the Determination of Phase from Image and Diffraction Plane Pictures. *Optik*, Vol.35 (No.2):237–246, 1972.

[37] Heinz H. Bauschke, Patrick L. Combettes, and D. Russell Luke. Phase retrieval, error reduction algorithm, and Fienup variants: a view from convex optimization. *J. Opt. Soc. Am. A*, 19(7):1334–1345, Jul 2002. doi: 10.1364/JOSAA.19.001334.

[38] J. R. Fienup and C. C. Wackerman. Phase-retrieval stagnation problems and solutions. *J. Opt. Soc. Am. A*, 3(11):1897–1907, Nov 1986. doi: 10.1364/JOSAA.3.001897.

[39] J. R. Fienup. Phase retrieval algorithms: a comparison. *Appl. Opt.*, 21(15):2758–2769, Aug 1982. doi: 10.1364/AO.21.002758.

[40] Changliang Guo, Shi Liu, and John Sheridan. Iterative phase retrieval algorithms. i: Optimization. *Applied Optics*, 54, 05 2015. doi: 10.1364/AO.54.004698.

[41] Isaac C.D. Lenton, Alexander B. Stilgoe, Timo A. Nieminen, and Halina Rubinsztein-Dunlop. OTSLM toolbox for Structured Light Methods. *Computer Physics Communications*, page 107199, 02 2020. doi: 10.1016/j.cpc.2020.107199.

[42] Teledyne FLIR. Grasshopper3 USB3 Model: GS3-U3-91S6M-C. `https://www.flir.eu/products/grasshopper3-usb3/?model=GS3-U3-91S6M-C&vertical=machine+vision&segment=iis`. Accessed: 2023-06-01.

[43] Alexander Franzen. ComponentLibrary, since 2006. URL `http://www.gwoptics.org/ComponentLibrary/`. Licensed under a Creative Commons Attribution-NonCommercial 3.0 Unported License Accessed: 2023-06-01.

[44] Mattias Ammitzböll. Pulsed Laser Beam Quality Assessment via Phase Retrieval, 2021. URL `http://lup.lub.lu.se/student-papers/record/9065001`. Accessed: 2023-06-01.

[45] Kuo Niu and Chao Tian. Zernike polynomials and their applications. *Journal of Optics*, 24, 12 2022. doi: 10.1088/2040-8986/ac9e08.

[46] B.E.A. Saleh, M.C. Teich. *Fundamentals of Photonics Part I: Optics*, chapter 3: Beam Optics, page 93. John Wiley & Sons, Inc., 2019. ISBN 9781119506867.

Appendix

The amplitudes of the applied Zernike polynomials and the retrieved aberrations as the coefficient of the decomposed Zernike polynomials that are used to generate the retrieved Zernike phase patterns in Table 4.2 are shown in the following figures.
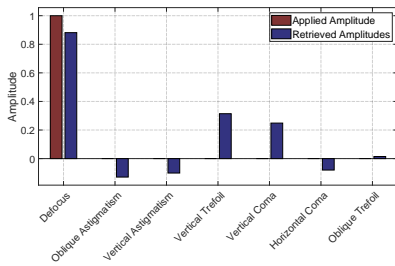

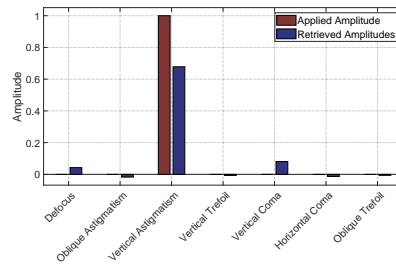**Figure 1:** Applied aberration: Defocus
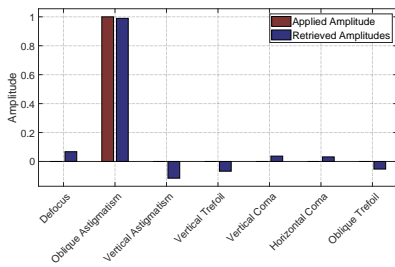

Figure 2: Applied aberration: Vertical Astigmatism
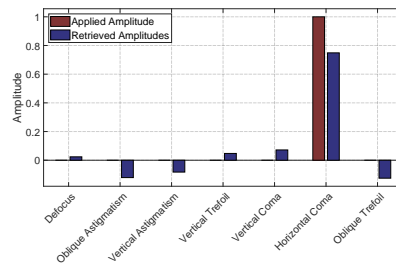

Figure 3: Applied aberration: Oblique Astigmatism

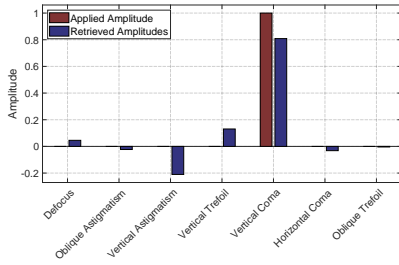**Figure 4:** Applied aberration: Horizontal Coma

Figure 5: Applied aberration: Vertical Coma
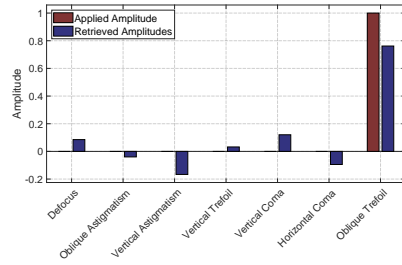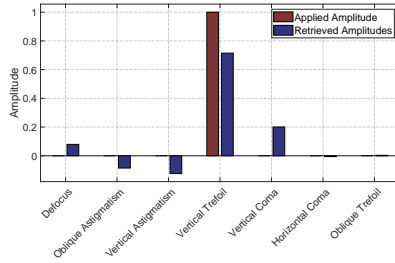

Figure 6: Applied aberration: Oblique Trefoil

Figure 7: Applied aberration: Vertical Trefoil